



HAL
open science

Stable isotope study of rainfall, river drainage and hot springs of the kerguelen archipelago, SW Indian Ocean

Renac Christophe, Bertrand N. Moine, Goudour Jean-Pierre, Leromancer Marc, Perrache Chantal

► **To cite this version:**

Renac Christophe, Bertrand N. Moine, Goudour Jean-Pierre, Leromancer Marc, Perrache Chantal. Stable isotope study of rainfall, river drainage and hot springs of the kerguelen archipelago, SW Indian Ocean. *Geothermics*, 2020, 83, pp.101726. 10.1016/j.geothermics.2019.101726 . hal-02326739

HAL Id: hal-02326739

<https://hal.science/hal-02326739>

Submitted on 21 Dec 2021

HAL is a multi-disciplinary open access archive for the deposit and dissemination of scientific research documents, whether they are published or not. The documents may come from teaching and research institutions in France or abroad, or from public or private research centers.

L'archive ouverte pluridisciplinaire **HAL**, est destinée au dépôt et à la diffusion de documents scientifiques de niveau recherche, publiés ou non, émanant des établissements d'enseignement et de recherche français ou étrangers, des laboratoires publics ou privés.



Distributed under a Creative Commons Attribution - NonCommercial 4.0 International License

1 Stable isotope study of rainfall, river drainage and hot springs of the
2 Kerguelen archipelago, SW Indian Ocean

3

4

5 Christophe Renac¹, Bertrand Moine², Jean-Pierre Goudour¹, Marc LeRomancer³ and Chantal
6 Perrache³

7

8 1. Géoazur (UMR 7329) Université de Nice Sophia-Antipolis, 250 Ave A. Einstein 06560
9 Valbonne France

10 2. Laboratoire Magma et Volcans (UMR 6524) Université de Saint-Etienne, 23 rue du
11 Dr. P Michelon 42023 Saint-Etienne France

12 3. LMEE (UMR 6197), Université de Brest, Technopôle Brest-Iroise - rue Dumont
13 d'Urville - 29280 Plouzané France

14

15 Corresponding author: christophe renac; email: renac@unice.fr; tel: (33) 04 83 61 85 61

16

17 Abstract

18

19 This study is the first synthesis of chemical composition and stable isotopes values for the
20 Kerguelen archipelago waters. The stable isotope values for rainfall and river waters in the
21 Kerguelen archipelago allow a calculation of the Local Meteoric Water Line ($\delta D_{\text{rainfall}} = 8.43$)

22 $\times \delta^{18}\text{O}_{\text{rainfall}} + 11$) and a summer runoff line ($\delta\text{D}_{\text{river drainage}} = 7.45 \times \delta^{18}\text{O}_{\text{river drainage}} + 6$).

23 Surface waters with low- ion concentrations, chlorine facies and stable isotope values

24 infiltrate through fractures and lava flows recharging deeper groundwaters. Thermal

25 groundwater with low- (7 to 50 °C) and high- (50 to 100 °C) temperatures emerges in

26 different localities in the volcanic archipelago. The low-temperature thermal waters might

27 represent a mixture of high-temperature water with rainfall, thermal gradient changes or

28 shallower infiltration compared to that for high-temperature thermal waters. The Rallier du

29 Baty and Val Travers areas contain geothermal fluids with high-temperature springs,

30 fumaroles and a large water flow. In the Rallier du Baty, the major ion chemistry and O, H, C

31 and S stable isotope ratio of low (7 to 50 °C) temperature spring waters in Rallier du Baty

32 area demonstrate a geothermal-system recharged by meteoric water ($\delta\text{D}_{\text{H}_2\text{O liquid}} = 7.0 \times \delta^{18}\text{O}_{\text{H}_2\text{O liquid}} + 0.5$) rather than sea water. The chemical and isotopic compositions of elevated

33 temperature spring waters (50 to 100 °C) have a long and complex history of meteoric water

34 interacting with cooling magmas ($\delta\text{D}_{\text{H}_2\text{O liquid}} = 1.78 \times \delta^{18}\text{O}_{\text{H}_2\text{O liquid}} - 23$). Surficial

35 precipitation of aragonite, kaolinite, pyrite, native sulfur attest to a long lived geothermal

36 system. A temperature of the geothermal reservoir has been estimated between 193 and 259

37 °C by cation geothermometry. The combination of minerals observed, major ion composition

38 of water with thermodynamic modeling and stable isotope data suggest a geothermal system

39 with a series of water/rock interactions from 50 to 250 °C. The conductive cooling of rising of

40 $\text{H}_2\text{O-CO}_2$ -rich fluids have produced a $\text{H}_2\text{O-CO}_2$ phase separation with the precipitation of

41 secondary minerals.

42

43

44 Keywords: Kerguelen archipelago, geothermal springs, stable isotope composition, water-

45 rock interaction

46

47 1 Introduction

48

49 A prolonged record of continuous magmatic activity has been documented for the Kerguelen
50 archipelago (Fig 1A; Giret, 1990; Weis and Giret, 1994; Weis et al., 1998; Mathieu et al.,
51 2011), but little attention has been paid to the type of hydrothermal system responsible for the
52 generation of hot springs and fumarolic activity. The volcanic archipelago of Kerguelen hosts
53 several geothermal centers expressed by continuous fumaroles and thermal springs (Fig. 1B to
54 E). Local rainfall and geothermal waters collected over the years by the permanent scientific
55 base and episodic fieldwork (1981 to 1983 and 2002 to 2009) allow a survey of chemical and
56 stable isotope values.

57 This survey involves of rainfall and fumarolic fields associated with thermal springs at
58 temperatures below the boiling point of water. Heat and fluid flow in these areas have been
59 related to a magmatic source releasing CO₂ (e.g., Delorme et al., 1994) and periods of
60 volcanism throughout the Kerguelen archipelago. However, there is a lack of observational
61 data cataloguing recent volcanic eruptions due to the remoteness of the Kerguelen
62 archipelago. Various authors have interpreted local magmatic petrogenesis and temperature in
63 the Kerguelen archipelago (Giret, 1990; Luyendick and Rennick, 1977; Weis and Giret, 1994;
64 Weis et al., 1998; Mathieu et al., 2011). Fewer authors have focused on seawater and meteoric
65 water exchanged by hydrothermal water/rock interaction of geothermal systems associated
66 with magma (Ballestracci and Nougier, 1984; Delorme et al., 1994; Verdier, 1989) and almost
67 very few papers deal with present-day hydrology (Berthois and Le Provost, 1971),
68 hydrogeology or geothermal fluids ($\delta^{13}\text{C}_{\text{CO}_2}$: Javoy et al., 1982).

69 Our studies reported in this paper present the first chemical and isotopic database for rainfall,
70 river drainage and thermal waters located in the Kerguelen archipelago. Stable isotope values
71 and the chemical composition will be used to “fingerprint” surface and geothermal water,
72 such as sources, recharge and transition processes taking place in underground aquifers such
73 as rainfall or seawater recharge and temperature changes (c.f. Barbieri, 2019; Wang et al.,
74 2018). We complemented the chemical composition and stable isotope values for fluids with
75 stable isotope values for minerals (kaolinite, aragonite, pyrite and native sulfur) precipitated
76 in thermal springs. Calculations based on stable isotope values for waters and minerals will be
77 used to estimate long-term or short-term changes in the composition of geothermal fluids.
78 Furthermore, magmatic and hydrothermal mineralogy combined with temperature estimates
79 of water/rock interaction has been implemented in a thermodynamic model. These
80 calculations have then been used for the Rallier du Baty area to schematize depth- mineral-
81 and fluid transformations from the deep groundwater-geothermal reservoir to the shallow
82 fumaroles and hot springs. The Kerguelen hydrothermal system provides a valuable dataset
83 for further comparative studies with the geothermal systems of Kerguelen or Iceland,
84 Guadeloupe, Hawaii and geothermal fields in the southern hemisphere.

85

86 Figure 1:

87

88 2 Regional setting

89

90 The Kerguelen archipelago is located in the southwestern Indian Ocean to the south of the
91 49th parallel. This archipelago plateau consists of successive submarine flows of tholeiite,

92 mildly alkaline basalts and trachyte associated with a silicic peralkaline volcanic activity
93 (Bonin et al., 2004; Weis and Giret, 1994) dated from 115 Ma to 39 Ma ago (Duncan, 2002;
94 Grégoire et al., 1997; Luyendick and Rennick, 1977). The emerged part of the archipelago
95 rises to 1850 m above sea-level (Fig. 1A) is a series of younger basalt flows and intercalated
96 ashes with ages ranging from 30 Ma to 0.13 Ma (Giret, 1990; Weis and Giret, 1994; Weis et
97 al., 1993, 1998; Gagnevin et al., 2003).

98 The rugged geomorphology (Fig. 1A) of the Kerguelen archipelago induces large rainfall
99 volumes in the west (estimated ca. 8000 mm/y) and drier conditions on the eastern side of the
100 island (~ 800 mm/y). This eastward difference relates to the Cook Ice Cap and Mount Ross
101 (Rallier du Baty area, RdB; Fig. 1B) with a permanent snow line at ca. 1200 m. This
102 mountainous system produces a cold and desertic climate with peat formation on the
103 archipelago. At the French weather station in Port aux Français (PaF: 49 ° 21'S; 70 ° 13'E;
104 Fig. 1A) the average daily temperature is 4.6 °C ±0.4 with 760 mm/y of rain (1951 to 2008:
105 data source Météo-France; cf. Lebouvier et al., 2011). Interpretation of satellite images taken
106 recently (cf. Berthier et al., 2009; Frenot et al., 1993; Vallon, 1977) suggests a glacial retreat
107 of 10 m/y. This ice retreat has been interpreted as related to current worldwide temperature
108 changes (Bergstrom et al., 2006; Smith, 2002) which in Port aux Français records +0.2 °C/y
109 and -10 mm/y of rain during the last twenty years. The large "Rivière du Chateau" watershed
110 shows seasonal flow changes from 1 to 25 m³/s and low dissolved solids content of waters.
111 The low dissolved solids content of the water is related to a significant proportion of melted
112 snow and rainfall rather than a contribution from sea sprays (Berthois and Le Provost, 1971).
113 The Scientific base of Port au Français (150 people during summer) uses drinkable water
114 from a river in the Loranchet area, while the hydrology and hydrogeology of the Kerguelen
115 (ca. 7215 km² with maximum 150 human being), is totally unknown.

116 The basaltic Kerguelen plateau hosts disseminated occurrences of altered tholeiitic lavas with
117 clay minerals, sulfide, silica precipitation, zeolite and carbonates (Delorme et al., 1994; Renac
118 et al., 2010; Verdier, 1989). The ‘Rallier du Baty’ (RdB) and ‘Presqu’îles de la Société de
119 Géographie’ (PSG; Fig. 1A) locations represent visible, modern and large hydrothermal areas
120 with a geothermal activity witnessed by fumarolic activity (Ballestracci and Nougier, 1984;
121 Gagnevin et al., 2003). The largest fumarolic area is located at 49 ° 37’S, 68 ° 47’E (Fig. 1B;
122 Ballestracci and Nougier, 1984); and the highest flow of thermal waters recognized in the Val
123 Travers (49 ° 19’ 41S, 69 ° 24’10E; Fig. 1C, Berthois and Le Provost, 1971; Delorme et al.,
124 1994).

125

126 3 Field measurements, water sampling, and chemical preparation

127

128 From 1981 to 1983 B. Blavoux and J. Nougier collected rainwaters (18 months) at the French
129 meteorological station of PaF (Table 1, unpublished data provided by Bernard Blavoux).
130 During summer camps (1981 to 1983) a series of river drainages and thermal springs
131 throughout the whole archipelago were sampled (Fig. 1A; Tables 1, 2, 3). A digital elevation
132 model and Qgis treatments associated these samplings (river drainage and springs) with tens
133 of small catchment areas (<1 km²) and a larger watershed (<30 km², Fig. 1 B to E). These
134 outlets are each other separated from 50 to 500 m (surface distance). Further scientific
135 programs from 2002 to 2009 (Carbonatoker Dylioker and Hotvir IPEV program) allow
136 summer sampling of river drainages, material from fumaroles, spring waters with low- to
137 high-temperatures at Rallier du Baty, the Central-Plateau and Gallièni. Hot springs emerge in
138 large ponds with thermal waters or as steam vents from fissures cutting lava flows or

139 pyroclastic rocks. Some outcrops and ponds are surrounded by centimeters to decimeters wide
140 muddy fringes of gray to red altered volcanic rocks.

141 Field measurements of fluid parameters consisted of pH, temperature ($^{\circ}\text{C}$), alkalinity (mg/L),
142 and electrical conductivity measurements ($\mu\text{S}/\text{cm}$). For each water locality, four bottles of
143 filtered water (250 cm^3) plus several blanks of ultrapure Millipore water (Saint Etienne, $\delta^2\text{H}=-$
144 -60‰ , $\delta^{18}\text{O}=-8.5\text{‰}$, $\delta^{13}\text{C}$ and $\delta^{34}\text{S}=\text{unmeasurable}$), with 1) Untreated waters for O, H
145 isotopes, anions, and alkalinity analyses. 2) Samples with $\sim 10\text{ cm}^3$ of 1% HNO_3) for cations
146 and $\delta^{34}\text{S}_{\text{SO}_4}$ analyses as BaSO_4 precipitates. 3) Water treated with 2 cm^3 of 20N NaOH liquid
147 ($\text{pH} > 12$) plus 5 cm^3 of a BaCl_2 saturated solution added to the basic water to allow the
148 precipitation of the dissolved species of carbon and sulfur as BaCO_3 and BaSO_4 . Further, each
149 precipitate was rinsed with deionized water and air-dried. The BaCO_3 and BaSO_4 were
150 subsequently used to determine $\delta^{13}\text{C}_{\text{DIC}}$ and $\delta^{34}\text{S}_{\text{SO}_4}$ values. 4) We analyzed samples from
151 two fumaroles at Rallier du Baty for $\delta^{13}\text{C}_{\text{CO}_2}$ values. Gases flowing through a quartz tube
152 were cooled and bubbled into NaOH to remove H_2O vapor and CO_2 . The CO_2 was
153 precipitated as BaCO_3 and analyzed for $\delta^{13}\text{C}_{\text{CO}_2}$. After tube purging and 30 min of steam
154 flow, we collected anhydrous gas on outgassed charcoal in Pyrex tubes sealed for transport
155 preservation and later analyzed for CO, N_2 and Ar proportions in the laboratories at the
156 University of St Etienne. The mineralogy of red and gray precipitates surrounding mineral
157 and thermal springs were characterized by X-ray diffraction (XRD; Brucker SIEMENS
158 D5000 Model with 40 kV and 25 mA, at Ecole des Mines de Saint-Etienne). Further, we
159 analyzed O, H (clays-minerals) and S (sulfide, native sulfur) stable isotopes of mono-mineral
160 separates with procedures presented in Renac et al. (2010).

161

163

164 In the laboratory (field 1981-1983, Blavoux analyst; 2002-2009 Renac and Perrache
165 analysts) analysis of cation-anion concentrations, O, H, C, and S stable isotope ratios were
166 added to field measurements. Water samples and blank water were transported and stored in
167 fridges and the following techniques of chemical analysis have been realized between 3 and 6
168 months after sample collection. For the first of the samples (1981 to 1983 mission)
169 inductively coupled plasma atomic emission spectroscopy (ICP-AES) was used for cation and
170 ion-specific electrodes for anion analysis for major element determinations at the Laboratoire
171 d'Hydrologie d'Avignon and Thonon Les Bains (unpublished data communicated by B.
172 Blavoux). While the ion composition of water samples, collected from 2002 and 2009, were
173 determined by DIONEX ion chromatography (cations: Na, Ca, Mg, K, Sr, Li; anions: F, Cl,
174 NO_3^- , SO_4^{2-} , Br, and PO_4^{3-} ; a detection limit 20 ppb and potential contamination related to the
175 transport and storing of blank of <0.1 ppm). Stable isotope ratios of oxygen were determined
176 using off-line extraction techniques with $\text{H}_2\text{O}-\text{CO}_2$ equilibration for oxygen isotopes
177 (Majoube, 1971). The hydrogen isotope ratio was measured on H_2 after water reduction by
178 hot depleted uranium (Bigeleisen et al., 1952). To obtain Carbon and sulfur stable isotopes
179 dissolved in water BaCO_3 (5 mg) was reacted with H_3PO_4 , to liberate CO_2 then analyzed for
180 carbon isotopes (McCrea, 1950). The S isotopes in dissolved sulfate were measured on SO_2
181 after combustion of BaCO_3 plus BaSO_4 precipitates (>350 μg) using a Vario Micro©
182 elemental analyzer equipped with an IR detector (2002- 2009 samples). Quality control
183 carried out on blank water indicate no $\delta^2\text{H}$, $\delta^{18}\text{O}$ and $\delta^{34}\text{S}$ changes, a small contamination by
184 atmospheric CO_2 (0.05 mg/250 ml) was observed and related to sample preparation (opening
185 addition of NaOH and BaCl_2 solutions) and transportation. This relatively low C

186 contamination, while water samples contain tens or hundreds milligram of carbonate species,
187 has been neglected in further carbon isotope interpretation.

188 We measured $\delta^{18}\text{O}_{\text{H}_2\text{O}}$, $\delta\text{D}_{\text{H}_2\text{O}}$, $\delta^{13}\text{C}_{\text{DIC}}$, $\delta^{34}\text{S}_{\text{SO}_4}$ values by double (1981 to 1983 samples:
189 VG602 E) and 2002 to 2009 samples on triple collectors (ISOPRIME) isotope ratio mass
190 spectrometers equipped with a dual-inlet and a continuous flow system for $\delta^{34}\text{S}$
191 measurements. All stable isotope values are reported as per mil (‰) relative to V-SMOW for
192 O and H in silicates and water (Coplen, 1988), $\delta^{34}\text{S}$ values relative to V-CDT and $\delta^{13}\text{C}$ values
193 relative to V-PDB. Analytical error and reproducibility for standards (NBS 18, NBS 19, NBS
194 123, NBS 127) and replicates are ± 0.05 ‰ for the $\delta^{13}\text{C}_{\text{BaCO}_3}$ equivalent of $\delta^{13}\text{C}_{\text{DIC}} \pm 0.2$ ‰
195 for $\delta^{34}\text{S}_{\text{BaSO}_4}$ and ± 0.1 ‰ for $\delta^{18}\text{O}$ of water, and ± 1 ‰ for δD (2δ) of water

196 We quantified the anhydrous gases collected on charcoal (Ar, N₂) with an ISOPRIME dual
197 inlet system. The mass calibration was realized on mass 36 for Ar mass 28 for N₂ and mass 44
198 for CO₂ and peak jumps. We measured the relative proportions of argon and nitrogen with a
199 calibration curve obtained with mixtures anhydrous gas (Ar/N₂: 0.9/78; 2/ 98; 10/90; 20/ 80).

200

201 5 Results

202

203 5.1 Rainwater and river drainage at Kerguelen.

204

205 Rainwater volume and temperature measured from 1981 to 1983 are similar to the recent data
206 obtained from the meteorological station at Port aux Français (PaF; Table 1). Meteoric waters
207 at Port aux Français have low-concentrations with dominant Na and Cl contents with a 1:1
208 Na/Cl molar ratio for temperatures between 1 and 12 °C (Table 1; Fig. 2A). The $\delta^{18}\text{O}$ rainfall

209 and δD rainfall values vary from -4 to -12 ‰ and -22 to -91 ‰ respectively. The most
210 negative O and H stable isotope values were associated with snow storms. These O and H
211 stable isotope values define a local meteoric water line (LMWL, $\delta D_{\text{rainfall}} = 8.43 \times \delta^{18}O_{\text{rainfall}}$
212 + 11, $R^2 = 0.975$; Σ rainfalls 1625 mm/ 18 months; Fig. 2B). The mean weighted $\delta^{18}O_{\text{rainfall}}$
213 value in 1982 was -6.8 ‰. River drainages dominantly in the southern part of the archipelago
214 are Na and Cl dominant (Table 2; Fig. 2A) with Na concentrations higher than rainfalls.
215 Moreover, the rivers are more Na- Cl-rich on the eastern side of the archipelago (Jeanne
216 d'Arc, Ronarc'h and Loranchet areas, Fig. 1A) than the western Rallier du Baty area (Table
217 1). The Oxygen and hydrogen stable isotope values of river drainages form a trend line
218 parallel to the local meteoric water line ($\delta D_{\text{river drainage}} = 7.45 \times \delta^{18}O_{\text{river drainage}} + 6$, $R^2 = 0.837$;
219 Fig. 2B).

220

221 Figure 2 and Tables 1 to 3

222

223 5.2 Geothermal localities

224

225 Thermal waters (from 7 to 100 °C) usually appear as isolated ponds. The RdB area hosts
226 many springs with a lower flow rate than in VT and Gallièni areas (Val Travers in the Plateau
227 Central; Fig. 1C). In the RdB area, many small ponds can be found within a few square
228 kilometers (Rallier du Baty; Fig. 3A). Thermal waters from rocks to ponds flow through
229 channels stained by iron oxides, and along clay-rich horizons (Fig. 3B) intercalated in lava
230 units associated with basaltic scoria (Fig. 3C). Some thermal outlets are surrounded by
231 precipitation of kaolinite (XRD: 1Md polytype), goethite, pyrite, and native sulfur (RdB). The
232 water temperature varies from an average surficial temperature of 6 to steam fumaroles at 100

233 °C. We arbitrarily define low-temperature springs as waters with temperatures higher than the
234 average surficial temperature (6 °C) up to a maximum of ~50 °C. This range of temperature
235 corresponds to a majority of thermal waters disseminated through the archipelago with
236 variable flow rates with traces of mineral precipitation (Infernet valley, Fallot glacier, and
237 Gallièni Massif; Table 3). The Val Travers area and the active fumaroles in the Rallier du
238 Baty (RdB) area have both low- (7 to 50 °C, Fig. 3D and E) and high- temperature waters (50
239 to 100 °C; Figs. 1A and 3F).

240 In the RdB area, thermal springs (7 to 100 °C) are distributed from mean sea level to an
241 altitude of 500 m above sea level (a.s.l.). Thermal water flow rates vary from 10s' L/ s (50 to
242 220 m) to low-flow rates represented by condensed H₂O liquid +H₂O vapor in a bubbling
243 oxide-rich ponds (ca. 1 L/ hour) located above 220 m. springs. The low-temperature thermal
244 waters occur from sea level to 220 m and high-temperature fluids (H₂O liquid + vapor and
245 CO₂; 97 °C, Fig. 3F) between 220 m and 450 m above sea level.

246

247 5.3 Chemical and isotopic compositions of thermal fluids and hydrothermal 248 precipitates

249

250 Low-temperature thermal waters, from sea level to 220 m, have dominant Ca, Mg, Na and
251 HCO₃⁻ ion compositions (Table 3) with neutral pH and rare springs with a basic pH (Fig. 3B).
252 The Na/Cl molar ratios are higher than those measured at rainfall river drainages (Fig. 4A).
253 Some of the low-temperature thermal waters have high-Ca, K, Mg, NO₃⁻, SO₄²⁻ and Br ion
254 contents with Na/Cl molar ratio < 1.9 below diluted seawater content and EC > 300 µS/cm
255 (Fig. 4A). These waters have been further described as mineral waters. The high- temperature
256 thermal waters (> 220 m above sea-level) have neutral to acid pH (~ 3), low EC and Total

257 Dissolved Solids (TDS; Table 3) with Na, Cl to Na, Cl, SO_4^{2-} ion concentrations and very
258 low-Na/Cl molar ratios.

259 Oxygen and hydrogen stable isotopic values of mineral and low- temperature thermal waters
260 (7 to 50 °C) plot on or beside the local meteoric water line and define a line ($\delta\text{D}_{\text{H}_2\text{O liquid}} = 7.0$
261 $\times \delta^{18}\text{O}_{\text{H}_2\text{O liquid}} + 0.5$; $R^2 = 0.904$) (LMWL). A large number of high- temperature thermal
262 waters (50 to 100 °C) are located on both sides of this LMWL. Nevertheless, some $\delta^{18}\text{O}$ and
263 δD values of high- temperature thermal waters form a trend line ($\delta\text{D}_{\text{H}_2\text{O liquid}} = 1.78 \times \delta^{18}\text{O}_{\text{H}_2\text{O liquid}}$
264 $- 23$, $R^2 = 0.65$; Fig. 4B) from LMWL toward more positive values of $\delta^{18}\text{O}$ and δD
265 values.

266 In low- and high- temperature thermal waters dissolved carbon and sulfur species define a
267 wide range of stable isotopic values. The low-temperature thermal waters have $\delta^{13}\text{C}_{\text{DIC}}$ and
268 $\delta^{34}\text{S}_{\text{SO}_4}$ values ranging from -5.6 to -23 ‰, and of +5 to +12 ‰, respectively (Table 3). The
269 spring having high-Ca, K, Mg, NO_3^- , SO_4^{2-} , and Br ion contents has the highest $\delta^{34}\text{S}_{\text{SO}_4}$ value
270 (11.6 ‰) and the lowest $\delta^{13}\text{C}_{\text{DIC}}$ value (-23 ‰). High-temperature thermal springs, with
271 lower TDS contents than low- temperature springs (7 to 50 °C), have $\delta^{13}\text{C}_{\text{DIC}}$ and $\delta^{34}\text{S}_{\text{SO}_4}$
272 values ranging from -5 to -10 ‰ and +3 to +9 ‰, respectively (Table 3).

273 The two steamers associated with high-temperature waters consist of H_2O vapor dominant
274 (approximately 95 %) with CO_2 ($\delta^{13}\text{C}_{\text{CO}_2} = -5.1 \text{ ‰} \pm 0.2$), and S-rich gas attested by the odor
275 and native sulfur in muddy deposits. The measured anhydrous gases in vapor dominant steam
276 have a total pressure lower than atmospheric pressure (0.09 MPa) with dominant N_2 (98.7 %)
277 minor Ar (1.2 %) and traces of He and CO (close to detection limit= 1 ppmv).

278 The X-ray diffraction of mineral precipitates in the zone of low-temperature springs (0 to 220
279 m) identified precipitates of aragonite (Fig. 3D) or amorphous silica and goethite (Fig. 3E).

280 The aragonite precipitation has an average $\delta^{13}\text{C}_{\text{aragonite}}$ of $+2.1\text{‰} \pm 0.3$ (Table 3). In the upper
281 zone with hot thermal water, a steam vent surrounded by mud consisted of dominant
282 kaolinite, mixed with euhedral pyrite. These euhedral pyrites (py) in this kaolinite-rich mud
283 have $\delta^{34}\text{S}_{\text{py}}$ between -2.3 and -1.5‰ ($n=5$ values) and a trace of native sulfur $+3.5\text{‰}$ ($\delta^{34}\text{S}$
284 native sulfur). The high-temperature thermal waters in ponds contain water mixed with
285 goethite and a smaller proportion of amorphous silica with kaolinite (kln) (Fig. 3F). The O
286 and H stable isotope values ($\delta^{18}\text{O}_{\text{kln}}$ and $\delta\text{D}_{\text{kln}}$) of kaolinite from the steam vent have of 20.8
287 ‰ and -91‰ respectively.

288

289 Figures 3 and 4

290

291 6 Discussion

292

293 6.1 Rainwater and river drainages

294

295 The Na-Cl composition for rainwater to surface water and river drainages covers a
296 large range of salinity ($5 < \text{Na} < 27$ mg/l). We associated the highest salinity to rainfall more
297 influenced by oceanic storms than the usual westward winds. These stormy conditions have
298 mixed seawater spray with rainfall. The stable isotope values for rainfall in the eastern
299 Kerguelen archipelago (PaF) draw the local meteoric water line (LMWL). However, the large
300 topographical change from the western to the eastern side of the island does not allow
301 extrapolation of these observations throughout the whole archipelago.

302 The river drainages during the summer are slightly more saline with O and H isotopes data
303 forming a restricted domain of values as rainfalls (Table 1, Fig. 2A). The increasing salinities
304 from West to East (Gallièni, Jeanne d'Arc, Ronarc'h and Loranchet plateau) suggest that
305 runoff is Na-enriched either by leaching of a Na-rich surface of rocks or by storms in the
306 eastern archipelago. We favor higher proportion of sea spray mixed with rainfall during storm
307 events considering the low-altitude of the eastern part of the archipelago. Whereas, mountains
308 on the western side of the archipelago reduce the inland incursion of storms as shown by the
309 western-side watershed basins (Fig. 1A).

310 The O and H stable isotope values of river drainages aligned and centered with the LMWL
311 confirm that they are meteoric water (rainfall and snowmelt: lowest $\delta^{18}\text{O}$ and δD) runoff and
312 can percolate throughout the Kerguelen volcanic plateaus. The river drainages from the
313 western side of the Archipelago (RdB) have the lowest Na-Cl concentrations, and similar to
314 slightly higher O-H stable isotope values (Table 2, Fig. 2B). We interpreted this data as
315 dominant meteoric waters with low salinity related to the dilution of sea spray by more rain
316 (orographic effect: estimated around 8000 mm per year on the western coast and 800 mm per
317 year on the Eastern side PaF).

318

319 6.2 Organic contamination of thermal water

320

321 Flowing thermal springs or larger geothermal areas in Rallier du Baty and Val Travers have
322 different recharge areas (Fig. 1B and 1C) and geothermal reservoirs. Each of these geothermal
323 areas may represent one or several sources of steam; high-temperature thermal water derived
324 from condensed steam and mixtures with meteoric water (e.g., Giggenbach and Stewart,
325 1982; Marini, 2004). Moreover, thermal springs (the Infernet Valley, Fig. 1B) located on the

326 coastline represent a nesting area for different penguin communities. The proximity of
327 animals at the low-altitude with low-temperature thermal springs of the Infernet Valley has
328 changed the composition of water with high-Ca, K, Mg, Cl, SO_4^{2-} ($\delta^{34}\text{S}_{\text{SO}_4}$: 11.6 ‰), NO_3^- ,
329 Br and HCO_3^- ($\delta^{13}\text{C}_{\text{DIC}}$: -23 ‰) ion concentrations with O and H stable isotope values lying
330 on the LMWL (PaF). These elementary constituents and stable isotope values show dominant
331 meteoric water with S species related to seawater and C species derived from organic matter
332 (Hoefs, 1980; Lowenstern et al., 1999). Consequently, we eliminated these springs from our
333 further geothermal interpretation and focused on area multiple emergences of thermal water
334 (Fig. 1A) in the Rallier du Baty and Val Travers areas. These areas host the highest
335 temperatures water (RdB), with high flow rates (VT).

336

337 6.3 Origin of 7 to 50 °C waters

338

339 We tried to identify the recharge of this hydrothermal system with O, H, C and S
340 stable isotope values of fluid and minerals. The 7 to 50 °C thermal springs are dominant in the
341 Kerguelen. These waters have O and H stable isotopes that define a line ($\delta\text{D}_{\text{H}_2\text{O liquid}} = 7.0 \times$
342 $\delta^{18}\text{O}_{\text{H}_2\text{O liquid}} + 0.5$; Fig. 4B) parallel to the river drainage (e.g., summer runoff: $\delta\text{D}_{\text{H}_2\text{O liquid}} =$
343 $7.45 \times \delta^{18}\text{O}_{\text{H}_2\text{O liquid}} + 6$) and LMWL (PaF). This parallel trend suggests a dominant
344 proportion of meteoric water in the low-temperature springs (Rallier du Baty, Plateau Central;
345 Gallièni) regardless of pH and chemical composition. Nevertheless, some of the $\delta^{18}\text{O}$ and δD
346 $\text{H}_2\text{O liquid}$ values do not fall on the line. Displacement of the $\delta^{18}\text{O}_{\text{H}_2\text{O liquid}}$ and the right side of
347 the LMWL might be related to water/rock oxygen exchange or a mixture of high-temperature
348 thermal water with a more positive $\delta^{18}\text{O}_{\text{H}_2\text{O liquid}}$ (see below) with rainfall or melted snow
349 (part. 5.1), localities with a lower thermal gradient or a similar thermal gradient at a shallower

350 infiltration than the high-temperature waters. However, the lack of a time series of analysis
351 did not permit the characterization of this phenomenon. In both cases, the meteoric recharge
352 would be driven by the topography and infiltration through fractures, or along discontinuities
353 between lava-flows and pyroclastic rocks (Fig. 3F). Their $\delta^{13}\text{C}_{\text{DIC}}$ and $\delta^{34}\text{S}_{\text{SO}_4}$ data (Table 3)
354 confirm dominant sources of inorganic carbon (magmatic- mantle= $-6.0\text{‰} \pm 1$; e.g., Javoy et
355 al., 1982) and sulfur (Hattori and Muehlenbachs, 1980; Watanabe and Sakai, 1983).
356 Moreover, the substantial precipitation of aragonite observed (Fig. 3D) with $\delta^{13}\text{C}$ values
357 recognized in hydrothermal systems (eg., Pichler and Veizer, 2004) suggests an even more
358 important proportion of inorganic CO_2 in the past than the present-day.

359

360 6.4 Origin of 50 to 100 °C waters

361

362 The high-temperature thermal waters and fumaroles are the most representatives of a
363 significant thermal flux or magma-derived fluids. The fluid flow of hot springs with thick
364 kaolinite precipitates suggest a long-lived period of fluid circulation. The other thermal
365 springs was not sufficient nor the composition stable enough for analysis. Therefore, the long-
366 lived flow, temperature, and chemistry was not estimated for other localities. This kaolinite
367 may have precipitated from fluids different from the present-day ones. Consequently, $\delta^{18}\text{O}$
368 $\text{H}_2\text{O liquid}$ (-5.1‰) and $\delta\text{D}_{\text{H}_2\text{O liquid}}$ (-39‰) in equilibrium with kaolinite were first calculated
369 (Savin and Lee, 1988; Sheppard and Gilg, 1996) with the present-day temperature of steam (T
370 measured= 97 °C ; Table 3). The calculated $\delta^{18}\text{O}_{\text{H}_2\text{O liquid}}$ and $\delta\text{D}_{\text{H}_2\text{O liquid}}$ are comparable to
371 present-day O-H stable isotope values ($\delta^{18}\text{O}_{\text{H}_2\text{O liquid}}$ measured: -4‰ ; $\delta\text{D}_{\text{H}_2\text{O liquid}}$ measured: -
372 32‰). Secondly, we used an equilibrium temperature of 105 °C (T measured = 97 °C) with
373 $\delta^{18}\text{O}_{\text{kln}}$ and $\delta\text{D}_{\text{kln}}$ of kaolinite (cf. paragraph 5.2) and its spring water ($\delta^{18}\text{O}_{\text{H}_2\text{O liquid}}$ = -4‰ ;

374 $\delta D_{H_2O \text{ liquid}} = -32 \text{ ‰}$). Both calculations prove the precipitation of kaolinite with H_2O_{liquid} with
375 $\delta^{18}O_{H_2O \text{ liquid}}$ and $\delta D_{H_2O \text{ liquid}}$ along the LMWL. The equilibrium of kaolinite with H_2O_{liquid}
376 indicates a minor isotope exchange between H_2O_{liquid} and vapor phases and small
377 temperature variations between past water, precipitating kaolinite, and present-day waters.

378 In the Val Travers area, the stable isotope ratios of the high-temperature thermal waters are
379 more negative ($\delta^{18}O$: -9.4 to -8.1 ‰ and δD : -58 to -50 ‰) than those of the RdB (Table 3)
380 and plot along the LMWL. The RdB high-temperature thermal waters have O, H stable
381 isotope values below the LMWL (PaF) and form a trend line ($\delta D_{H_2O \text{ liquid}} = 1.78 \times \delta^{18}O_{H_2O}$
382 $_{\text{liquid}} - 23$) with an intercept with the LMWL at $\delta^{18}O_{H_2O \text{ liquid}} \sim -5 \text{ ‰} \pm 1$ and $\delta D_{H_2O \text{ liquid}} \sim -35$
383 ‰ and equivalent to a fluid in equilibrium with kaolinite. This intercept value is higher than
384 those from river drainage or low-temperature thermal waters. In similar geothermal contexts,
385 this intercept of thermal water lines and the LMWL represents the meteoric-water recharge of
386 the geothermal field (cf. Clayton et al., 1968; Clayton and Steiner, 1975; Craig et al., 1956,
387 Fritz and Fontes, 1986; Truesdell and Hulston, 1980).

388 Whatever the $\delta^{18}O$ and δD position on the LMWL, this meteoric recharge excludes the
389 infiltration of seawater, located few kilometers away, in the geothermal reservoir. This
390 meteoric recharge is in agreement with the low-salinity of all thermal springs in the Kerguelen
391 archipelago. The meteoric recharge in the RdB area is delimited by a watershed in the
392 surrounding volcanic plateaus with an average altitude of 700 m a.s.l. (Figs. 1B and 2) and the
393 permanent snow line at a maximum altitude of ~1200 m (Table 2). Consequently, the higher
394 $\delta^{18}O$ and δD values of the intercept suggests, a meteoric water recharge less influenced by
395 melted snow than river drainage or a similar recharge affected by additional processes such as
396 vapor-condensed liquid separation (Giggenbach and Stewart, 1982), H_2S - CO_2 - H_2O isotope
397 exchange, and water-rock interaction (reference aforementioned). These processes are

398 evidenced by the composition of fumarole steam with anhydrous gas and an N₂/ Ar molar
399 ratio of 80, similar to that of atmospheric air (84; cf. Fischer et al., 1998; Giggenbach, 1995;
400 Shaw et al., 2003), as well as the inorganic carbon ($\delta^{13}\text{C}_{\text{CO}_2} = -5.1 \text{‰} \pm 0.2$) and the native
401 sulfur ($\delta^{34}\text{S}_{\text{native sulfur}} = 3.5 \text{‰}$; Table 3; e.g., Craig, 1963; Javoy et al., 1982; Hoefs, 1980;
402 Lowenstern et al., 1999). These additions of gas through hydration may contribute to an
403 increase in the proportion of sulfuric and carbonic acids (Ohmoto and Rye, 1979) and kinetic
404 water/rock interaction (Fritz and Fontes, 1986; Giggenbach, 1991; Liebscher and Heinrich,
405 2007).

406

407 6.5 Process changing stable isotope compositions of high-temperature of thermal 408 waters

409

410 In the RdB hydrothermal systems, condensed fumarole steam (steamers: $\delta^{18}\text{O}_{\text{H}_2\text{O vapor}} = +3 \text{‰}$
411 and $\delta\text{D}_{\text{H}_2\text{O vapor}} = -20 \text{‰}$; Table 3) is O and D enriched compared to fluids from other high-
412 temperature springs (Fig. 4B). The calculated $\delta^{18}\text{O}_{\text{H}_2\text{O liquid}} (2.24 \text{‰})$ and $\delta\text{D}_{\text{H}_2\text{O liquid}} (-7.8 \text{‰})$
413 values in equilibrium (oxygen and hydrogen fractionation factors; Majoube, 1971; Horita and
414 Wesolowski, 1994; Table 2) with these vapors for a temperature of 100 °C are more positive
415 than that of the estimated meteoric recharge ($\delta^{18}\text{O}_{\text{H}_2\text{O liquid}} \sim -5 \text{‰} \pm 1$ and $\delta\text{D}_{\text{H}_2\text{O liquid}} \sim -35 \text{‰}$;
416 part. 6.4). This calculation suggests either a different recharge or a vapor-liquid separation
417 associated with a stable isotopes kinetic-exchange.

418 This kinetic exchange can be estimated looking at the slope of $\delta^{18}\text{O}_{\text{H}_2\text{O}}$ and $\delta\text{D}_{\text{H}_2\text{O}}$ values for
419 high-temperature springs with a dominant H₂O- liquid in RdB. The trend line with $\delta\text{D}_{\text{H}_2\text{O}}$
420 liquid/ $\delta^{18}\text{O}_{\text{H}_2\text{O liquid}}$ with a slope of 1.78 then integrates buoyancy and changing vapor/liquid

421 ratios from depth to atmospheric pressure. The calculated $\delta D_{H_2O \text{ liquid}} / \delta^{18}O_{H_2O \text{ liquid}}$ ratio,
422 equivalent to the $\delta D_{H_2O \text{ liquid-vapor}} / \delta^{18}O_{H_2O \text{ liquid-vapor}}$ ratio, is lower than the predicted ratio
423 obtained by equilibrium or kinetic evaporation at ≤ 100 °C (below 100 °C: equilibrium= 5.3,
424 Majoube 1971 and kinetic evaporation= 2 to 5, Dansgaard 1964; Gonfiantini et al. 1973; Fig.
425 4B). This $\delta D_{H_2O \text{ liquid}} / \delta^{18}O_{H_2O \text{ liquid}}$ ratio below 2 exclude the equilibrium and kinetic process
426 of liquid- vapor separation below < 100 °C. These O and H stable isotope changes may also
427 relate to (i) isotopic fluid exchange (CO_2 , H_2S , and H_2O), ii) fluid/ rock interaction with O-H
428 isotopic exchange (Craig et al. 1956), iii) Mixing of meteoric water and magmatic-like water
429 (cf. $\delta^{18}O = +9$ to $+10$ ‰ and $\delta D = -8$ to -18 ‰; Giggenbach, 1992b).

430 Firstly, we established a conceptual model that considers the lower part of the RdB reservoir
431 as a rock-dominated system and the upper part of the reservoir with a steam dominated cell
432 (Giggenbach, 1992b). We examined, the CO_2 , H_2S and H_2O interactions able to produce
433 dominant “horizontal” ^{18}O shifts (cf. Giggenbach, 1992a) related to a CO_2 - H_2O oxygen
434 isotopic exchange (Majoube, 1971) and a H_2S - H_2O H isotopic exchange (cf. Galley et al.,
435 1972). In both cases, the low- CO_2 (measured $CO_2 < 5$ wt. %) and estimated H_2S proportion
436 (H_2S odor) and their C and S isotopic values would not produce an ^{18}O shift as observed
437 (Table 3; Fig. 4B; cf. Chiodini et al., 1993; Giggenbach, 1987).

438 The second hypothesis (i), $\delta^{18}O$ and δD on both above and below of the LMWL may
439 represent vapor and condensed liquid separation. The oxygen and hydrogen stable isotope
440 values of condensed liquid on the LMWL and vapor above the LMWL (Fig. 4B) with a δD
441 $\delta D_{H_2O \text{ liquid}} / \delta^{18}O_{H_2O \text{ liquid}}$ ratio of 1.78 would represent a high-temperature H_2O liquid-vapor
442 system at ~ 250 °C with a phase separation probably occurring in ascending fluids. Finally,
443 hypotheses ii) and iii) are difficult to separate since water/rock interaction may produce large
444 O isotope shifts driven by a thermal meteoric fluid/ magmatic rock interaction (Craig et al.,

445 1956). The stable isotope values tend toward this large domain so-called “magmatic-like
446 water” (cf. Capasso et al., 1997; Chiodini et al., 2000; Giggenbach, 1992b). In this case, the
447 hydrothermal alteration may shift the $\delta^{18}\text{O}_{\text{H}_2\text{O liquid}}$ and $\delta\text{D}_{\text{H}_2\text{O liquid}}$ toward the field of
448 magmatic-like water. However, no high-temperature hydrothermal mineral (K-feldspar,
449 epidote) has been observed in the RdB area.

450 We also calculated temperatures derived from different S isotopes in SO_4^{2-} -rich water and
451 pyrite (S-isotopes fractionation factor: Ohmoto and Rye, 1979; Robinson, 1973). Assuming
452 equilibrium, the calculation of $\delta^{34}\text{S}_{\text{SO}_4^{2-}} - \delta^{34}\text{S}_{\text{pyrite}}$ suggest a temperature varying from 240 to
453 300 °C. This calculation indicates either an inappropriate assumption of equilibrium or hot-
454 springs with a fluctuation of temperature (dominant kaolinite ca. 100 °C, minor pyrite 240 to
455 300 °C). For a similar assumption of equilibrium, the C stable isotope values of CO_2 gas and
456 CO_3^{2-} - rich water (C isotope fractionation factor: Mook et al., 1974). CO_2 and HCO_3^-
457 equilibrium would be between 50 and 115 °C. The range of calculated temperatures indicate
458 temperatures varying from 300 to 50 °C, with phase separation to water/rock interaction.

459

460 6.6 Ion concentration ternary diagrams and cation thermometers for water

461

462 The temperature range of the RdB geothermal reservoir was bracketed by the major
463 element composition. The large surface of this geothermal area is attested by the volcanic
464 context of the archipelago, and warm soils in the Infernet valley (Fig. 1B), where thousands of
465 animals breed. This thermal flux could be regional or a local convective heat flux
466 (Ballestracci and Nougier, 1984). The calculated critical points of water (NaCl between 0.001
467 and 0.1 weight %; CO_2 varying from 1 to 10 weight %; Table 2) between 340 and 370 °C for

468 22 MPa to 23 MPa (Duan and Sun, 2003) will limit the maximum temperature of the hydrous
469 geothermal reservoir.

470 The low- to high-temperature springs tend to have low- Na -Cl for acid and sulfate-rich
471 thermal waters. These chemical compositions may be the consequence of several processes
472 and the geometry of the geothermal reservoir. Processes can be due to hydrothermal cells with
473 steam or condensed steam (e.g., Giggenbach and Stewart, 1982; Marini, 2004), mixtures of
474 low-Na rainfall with a Na-precipitating phase, SO_4^{2-} enrichment for low Cl concentrations
475 with water-rock interaction (cf. Hedenquist et al., 1994; Sheppard, 1986; Taylor, 1979), and
476 up-flow circulation (Giggenbach, 1988).

477 We estimated the temperatures of the geothermal reservoir with a cation thermometer. The
478 calculated temperatures assume a chemical equilibrium between water and mineral in the
479 geothermal reservoir (e.g., Bowers and Taylor, 1985; Fournier and Potter, 1982; Pope et al.,
480 1987; Giggenbach, 1988; Fournier, 1991; Simsek and Gülec, 1994; White et al., 1971).

481 Thermal springs with steam loss with CO_2 , acid pH, or amorphous silica, kaolinite, and
482 aragonite indicate under-saturation or saturation of carbonates and silicates during conductive
483 undercooling or fluid transport. These conditions exclude the assumption of chemical
484 equilibrium for Si, Ca compounds and the use of Si-Ca geothermometry.

485 Consequently, a preliminary calculation of the temperature of the thermal reservoir used
486 information on conservative elements such as cationic diagram and thermometry (Fig. 5A;
487 Giggenbach, 1988). Nevertheless, the cation diagram shows that most low and high-
488 temperature spring waters are not classified as “fully equilibrated mineral waters” (Arnórsson,
489 2000; Arnórsson et al., 1983; Giggenbach, 1988). One acid and two basic thermal fluids plot
490 in the field of fully equilibrated water. A Cl^- , SO_4^{2-} and HCO_3^- diagram (Fig. 5B) and the
491 SO_4^{2-} -rich water suggest of volcanic origin; whereas the HCO_3^- -rich waters are reported in
492 the literature as related to peripheral waters or mature fluids.

493 Consequently, several cation thermometers have been used to estimate the temperature at
494 different stages of fluid/rock interaction. The calculation of Na- K cation thermometer
495 temperature is based on the water/feldspar interaction (Fournier and Truesdell, 1974). This
496 cation thermometer indicates that the two fully equilibrated waters considered in this study
497 would range from 270 to 290 °C (Fig. 5A). This range of temperature is similar to the one
498 obtained with high -temperature liquid-vapor ($\delta D_{H_2O \text{ liquid}} / \delta^{18}O_{H_2O \text{ liquid}}$ ratio= 1.78), sulfate-
499 pyrite equilibrium (240 to 300 °C).

500

501 6.7 Thermodynamic modeling of water/rock interaction in Rallier du Baty

502

503 Whole fluid-rock interaction and associated chemical changes have been reconstructed
504 with the thermodynamic model (PhREEQC 3.3 software, with the Lawrence Livermore
505 National Laboratory thermodynamic database: LLNL database, July 2017; Parkhurst and
506 Appelo 1999). We selected chemical compositions of the thermal spring waters in the fully
507 equilibrated field (Fig. 5A) with an estimated temperature of the geothermal reservoir
508 between 200 and 300 °C (Table 2). This model uses the influx of meteoric water with a
509 chemical composition of river drainage in RdB (Cap Bourbon) representing the meteoric and
510 hydraulic recharge of the geothermal reservoir (Table 1). This meteoric recharge can interact
511 with the anorthite, albite, olivine, Ca-pyroxene, pyrite, and quartz for volcanic glass,
512 considered a primary mineral of the surrounding rocks (Beaux, 1986; Moine et al., 2004), and
513 produce secondary minerals observed in the RdB area (goethite, amorphous silica, aragonite,
514 kaolinite, and pyrite) or found in the Kerguelen archipelago (analcime, clinoptilolite, stilbite,
515 illite, smectite, quartz, K-feldspar (adularia) and carbonates; cf. Renac et al., 2010; Verdier,
516 1989).

517 This modeling assumes a first stage with the injection of meteoric water into a geothermal
518 reservoir where reactions reach equilibrium. The second stage will examine chemical changes
519 in fluids produced from the geothermal reservoir toward the surface. Temperature and
520 pressure in the first stage vary from 6 °C to a maximum temperature of 306 °C and from
521 atmospheric pressure to 24 MPa. In order to follow chemical changes 6 cells with a dT/dP
522 gradient of +50 °C/ +4 MPa were separated. In summary, a calculation with increasing
523 temperature and pressure predicts the dissolution of ferromagnesian minerals, feldspars in
524 trachyte and the production of a Na, Ca, H₂S and SO₄²⁻ acid brine (pH~ 4.5) well known to
525 exist in oceanic hydrothermal areas (Brombach et al., 2000; D'Amore and Panichi, 1980;
526 Pope et al., 2009). Such fluids in RdB and VT would represent the most thermal and pristine
527 geothermal fluids. Nevertheless, acid thermal waters represent a small number of recognized
528 hot springs in the Kerguelen archipelago (Table 3). The results of these calculations combined
529 with stable isotope values indicate that the analyzed geothermal waters have evolved
530 chemically. Consequently, the high -temperature H₂O liquid-vapor or CO₂ -HCO₃⁻ represent a
531 phase change and a separation during fluid ascent from the geothermal reservoir to the surface
532 (adiabatic cooling). This modeling predicts the formation of secondary minerals (smectite,
533 smectite-illite below 200 °C, quartz and K-feldspar (adularia) from 150 to 306 °C) that
534 haven't been recognized in the RdB or VT areas but described by Verdier (1989) in highly
535 altered rocks.

536 The second stage of this thermodynamic model deal with ascending fluids and mineral
537 changes from the geothermal reservoir (306 °C) through conductively cooling trachyte (50 to
538 100 °C). As observed, the calculation predicted the alteration of a primary mineral and the
539 precipitation of kaolinite (stable isotopes ca. 100 °C) and amorphous silica (Fournier and
540 Rowe, 1966) with pyrite at temperature starting at 150 °C. These secondary minerals
541 equilibrate with acid pH, a low-Si concentration with high-Na-Ca and SO₄²⁻ concentrations.

542 The low-Na concentration of the thermal waters suggests the precipitation of Na-rich
543 secondary minerals (zeolite or smectite).

544 The differences between the analyzed composition of the thermal waters and the calculated
545 composition combined with the interpretation of $\delta^{18}\text{O}$, δD , $\delta^{13}\text{C}$ and $\delta^{34}\text{S}$ values suggest that
546 the RdB area consists either of several hydrothermal cells (heated groundwater) and/or a
547 progressive separation of fluids (H_2O liquid-vapor, cation-anion changes, CO_2 dissolved -gas)
548 takes place. The $\delta^{18}\text{O}$ and δD hypothesis of an 'incomplete water-rock interaction' would be
549 derived from several hydrothermal cells with different liquid-vapor separation as suggested by
550 a SO_4^{2-} -rich water related to volcanic-sourced steam (part 6.3).

551 We combined these different hypotheses in a schematic cross-section in the RdB (Fig. 6).
552 This cartoon indicates a high-temperature geothermal reservoir with acid brine and water-rock
553 interaction between 250 and 300 °C. The final stage is represented by a CO_2 gas- HCO_3^- phase
554 separation (50 °C) associated with an N_2/Ar ratio similar to the atmospheric ratio. Between
555 these two stages, conductive cooling of rising fluids has produced carbonates, amorphous
556 silica, and kaolinite (~ 100 °C). The depth of the RdB geothermal reservoir is difficult to
557 determine because of the unknown geothermal gradient. Therefore, the meteoric origin of the
558 water recharging the RdB hydrothermal system (surrounding plateau: 700 to 1200 m, Fig. 1)
559 promotes a maximum hydraulic pressure of 7 to 12 MPa. Assuming a maximum pressure of
560 about 23 MPa (critical point of liquid water) then their differences would represent the
561 hydrostatic pressure below sea level. The difference ranges between 16 (23-7 MPa) and 11
562 (23-12) MPa equivalent to a depth of 1.6 km to 1.1 km or 0.4 to 0.6 km under hydrostatic or
563 lithostatic pressure. In such a context, the RdB geothermal gradient (300 °C/ 0.4 km or 300
564 °C/0.6 km or 300 °C/ 1.1 km or 300 °C/1.6 km) is equivalent to the Iceland or Guadeloupe
565 active geothermal fields (Pope et al., 2009; Brombach et al., 2000).

566

567 Figures 5 and 6

568

569 7 Summary and conclusions

570

571 The results of the comparison of chemical composition and stable isotope values for
572 rainwater, river drainage, minerals, and thermal spring waters supports the concept of
573 meteoric recharge and geothermal activity. The large volcanic plateau with issuing low- to
574 high- thermal waters in the different areas of the Kerguelen suggest that heated groundwater
575 might represent shallow and deep fluids and thermal water diluted with meteoric recharge.
576 Nevertheless, the fumarole field of Rallier du Baty and other geothermal locations in the
577 Kerguelen archipelago represent the surficial expression of meteoric-water hydrothermal
578 systems. In the Rallier du Baty, meteoric thermal waters are chemically modified by boiling
579 and gas-water-rock interaction. Meteoric recharge and thermal fluids such as acid brines have
580 interacted with anhydrous gas from magma to alter igneous rocks and to precipitate kaolinite
581 (ca; 100 °C), amorphous silica, carbonate on the surface and presumably adularia and zeolite
582 at depth.

583 The O, H and S stable isotope ratios confirmed a high-enthalpy hydrothermal system with
584 temperatures between 250 to 300 °C and HCO₃⁻ separation to CO₂ between 50 and 115 °C
585 associated with an N₂/Ar- like atmospheric ratio gas and the precipitation of kaolinite. The
586 depth of 400 to 1600 m below sea level of the geothermal reservoir was calculated using
587 values for lithostatic and hydrostatic pressure.

588 The stable isotope and chemical data presented in this paper could encourage further
589 comparisons to be made with infrared thermography, and fluid-inclusion microthermometry

590 to obtain a realistic interpretation of earlier magmatic activity in the simulation of active
591 geothermal systems throughout the Kerguelen archipelago.

592

593 Acknowledgments

594

595 We express our appreciation to the IPEV technical staff for logistic support, and to Guillaume
596 Delpech, and François Nauret who assisted us with fieldwork in the Kerguelen archipelago. In
597 memoriam Bernard Blavoux (†). He gave us (2011) data on samples collected in 1981 and
598 1983. We are grateful for the financial support provided by CARBONATOKER (2002),
599 DYLIOKER (2008) and HOTVIR (2009) programs. We especially thank Chris Bromley, Eva
600 SHILL (Editor-in-Chief of GEOTHERMICS), anonymous reviewers, J. Arigault-Rivera,
601 Peter Bowden, Guillaume Duclaux and anonymous reviewers for improving the English
602 grammar, Qgis tips, and the structure of the scientific text in this paper.

603

604 Figure and Table captions

605

606 Figure 1: A) Kerguelen Archipelago with locations of present-day hot springs (red dots:
607 Rallier du Baty, Plateau Central, Galliéni) and sampled river drainage (blue dots) associated
608 with a large watershed basin identified by a digital elevation model (SRTM 1arc second) and
609 QGIS software associated with flow accumulation, successive flow routing and catchment
610 area algorithms to delimit watersheds (Saga algorithms). B) a simplified geological map of
611 Rallier du Baty area, associated with a digital elevation model. C) A digital elevation model
612 of the Plateau Central area with Val Travers, Lili, Bossière thermal springs and watershed; D)
613 digital elevation model of the Jeanne d'Arc area with locations of sampled rivers and their

614 watersheds; E) digital elevation model of the Gallièni area with sampling locations of river
615 and thermal springs and watershed associated.

616

617 Figure 2: A) Na vs. Cl concentration (mg/l) of rainfall (red circle) and watershed waters (blue
618 circle) B) δD vs. $\delta^{18}O$ diagram, showing the isotope composition of rainwater from Port aux
619 Français and river drainage composition from all over the archipelago. Also, shown in A)
620 Na/Cl molar ratio distribution and composition of water mixed with seawater (diluted
621 seawater) as well as a Na vs. Cl regression line. In B) the worldwide and local meteoric water
622 lines are presented (Global meteoric water line: GMWL; Craig, 1961), the composition of
623 seawater and “andesite type magmatic waters” (Giggenbach, 1992a) regression line for the
624 local meteoric water line (LMWL) and river drainage regression line.

625

626 Figure 3: A) Fumarole field of Rallier du Baty (420 m a.s.l.), B) Thermal water iron oxides
627 and silica particles in the Upper Infernet valley, C) Steam and thermal water emergence in an
628 altered pumice level at the Infernet valley in the Rallier du Baty area, D) aragonite crust
629 encountered nearby low-temperature thermal springs in Plage du Feu de Joie E) modern opal
630 precipitates on Plage du Feu de Joie, F) Steamer sampled at Mount des fumarole for fluids
631 (H_2O and CO_2 , anhydrous gas) and alteration phases (kaolinite and pyrite).

632

633 Figure 4: A) Na vs. Cl concentration (mg/l) of mineral and thermal spring waters of
634 Kerguelen (7 to 50 °C: blue circle; 50 to 100 °C red circle); B) δD vs. $\delta^{18}O$ diagram, showing
635 the isotope composition 7 to 50 °C (blue circle) and 50 to 100 °C (red circle) of mineral and
636 thermal spring waters of the Kerguelen archipelago. Springs with carbonate, opal, kaolinite
637 precipitates are marked. Also shown are the GMWL (dashed line), the composition of

638 'andesite type magmatic waters' (Giggenbach, 1992) and Na, Cl and O-H stable isotope
639 composition of RdB watershed water A trend line for O- H stable isotope values is shown for
640 50 to 100 °C spring waters from the RdB (plain line).

641

642 Figure 5: Mineral and thermal water composition of Kerguelen (blue circle: 7 to 50 °C waters;
643 red circles: 50 to 100 °C waters and composition fields for rainwater and watershed waters) in
644 A) Na–K–Mg^{1/2} triangular diagram, and B) SO₄²⁻–HCO₃⁻–Cl (%) triangular diagram and
645 fields of immature and fully equilibrated waters as well as some calculated temperatures using
646 Na-K and Mg-K geothermometers (after Giggenbach 1988).

647

648 Figure 6: Schematic model of the Rallier du Baty geothermal field based on interpretations of
649 the water chemistry and stable isotope values. The model presents infiltration of meteoric
650 water into the geothermal reservoir followed by the upflow conductive cooling and a liquid-
651 vapor separation.

652

653 Table 1: Sampling of rainwater (month), average temperature, amount of rainfall (mm), ,
654 electrical conductivities (μS/cm), pH, total dissolved species (mg/l), chemical composition
655 (concentrations in mg/l), calculated amount of HCO₃⁻ (mg/l), and stable isotope values (δD
656 and δ¹⁸O) of rainwater in Port aux français (n.d. not detected; n.a. not analyzed)

657

658 Table 2: Location, GPS position and altitude of sampled river drainage in the Kerguelen
659 archipelago (Rallier du Baty, Val Travers, Galliéni, Ronarc'h...) with temperatures (°C),

660 electrical conductivities ($\mu\text{m}/\text{cm}$), pH, cation and anion concentrations (mg/L) and $\delta^{18}\text{O}$ - δD
661 stable isotope values.

662

663 Table 3: Location, GPS position and altitude of thermal and mineral springs in the Kerguelen
664 archipelago (Rallier du Baty, Val Travers, Galliéni, Ronarc'h...) with temperatures, pH,
665 alkalinities, electrical conductivities, cation and anion concentrations (mg/L), $\delta^{18}\text{O}$, δD ,
666 $\delta^{13}\text{C}_{\text{DIC}}$ or CO_2 and $\delta^{34}\text{S}_{\text{SO}_4}$ values (n.a. stands for not analyzed). The Na-K thermometer was
667 used to calculate the equilibrium temperature of water at the following conditions:
668 temperature above 50 °C, pH= 6.9 to 7.5; Ca/ Na molar ratio <1 and $\text{pCO}_2 < 10^{-4}$ atm

669

670 [References](#)

671

672 Arnórsson, S., (Ed.) 2000. Isotopic and chemical techniques in geothermal exploration,
673 development and use. Sampling methods, data handling, interpretation, International Atomic
674 Energy Agency, Vienna, 351 pp

675

676 Arnórsson, S., Gunnlaugsson, E., Svavarsson, H., 1983. The chemistry of geothermal waters
677 in Iceland. III. Chemical geothermometry in geothermal investigations. *Geochim.*
678 *Cosmochim. Acta.* 47, 567-577.

679

680 Ballestracci, R., Nougier, J., 1984. Detection by infrared thermography and modelling of an
681 ice-capped geothermal system in Kerguelen Archipelago. *J Volc Geotherm Res.* 20, 85-100.

682

683 Barbieri, M. 2019. Isotopes in Hydrology and Hydrogeology. *Water* 2019, 11(2), 291;
684 <https://doi.org/10.3390/w11020291>

685

686 Beaux, J.F., 1986. Le complexe volcano-plutonique de la Presqu'île de la Société de
687 Géographie (Iles Kerguelen) structure et pétrologie. PhD Thesis, Univ. Paris VI, 203 p

688

689 Bergstrom, D.M., Convey, P., Huiskes, A.H.L., 2006. Trends in Antarctic terrestrial and
690 limnetic ecosystems: Antarctica as a global indicator. Springer, Netherlands. Bergstrom,
691 D.M.; Convey, P.; Huiskes, A.H.L. (Eds.) XIV, 369 p

692

693 Berthier, E., Le Bris, R., Mabileau, L., Testut, L., Rémy, F., 2009. Ice wastage on the
694 Kerguelen Islands (49 °S, 69 °E) between 1963 and 2006. *J. Geophys. Res.* 114, F03005,
695 doi:10.1029/2008JF001192.

696

697 Berthois, L., Le Provost, C., 1971. Contribution à l'étude de la rivière du château : Presqu'île
698 Courbet – Archipel de Kerguelen. *Sciences Agronomiques Rennes* 23 p

699

700 Bigeleisen, J., Perlman, M.L., Prosser, H.C, 1952. Conversion of hydrogenic materials to
701 hydrogen for isotopic analysis. *Anal. Chem.* 24, 1356–1357.

702

703 Bonin, B., Ethien, R., Gerbe, M- C., Cottin, J- Y., Féraud, G., Gagnevin, D., Giret, A.,
704 Michon, G., Moine, B., 2004. The Neogene to recent Rallier-du-Baty nested ring complex,
705 Kerguelen Archipelago (TAAF, Indian Ocean): stratigraphy revisited implications for
706 cauldron subsidence mechanisms. *Geol. Soc. London Spec. Publ.* 234, 125–149.

707

708 Bowers, T.S., Taylor, H.P. Jr., 1985. An integrated chemical and stable isotope model of the
709 origin of midocean ridge hot spring systems. *J. Geoph. Res.* 90, 12583-12606.

710

711 Brombach, T., Marin, I.L., Hunziker, J.C., 2000. Geochemistry of the thermal springs and
712 fumaroles of Basse-Terre Island, Guadeloupe, Lesser Antilles. *Bull Volcanol.* 61, 477–490.

713

714 Capasso, G., Favara, R., Inguaggiato, S., 1997. Chemical features and isotopic composition of
715 gaseous manifestations on Vulcano Island, Aeolian Islands, Italy: an interpretative model of
716 fluid circulation. *Geochim. Cosmochim. Acta.* 61 (16), 3425-3440.

717

718 Chiodini, G., Allard, P., Caliro, S., Parello, F., 2000. ^{18}O exchange between steam and
719 carbon dioxide in volcanic and hydrothermal gases: Implications for the source of water.
720 *Geochim. Cosmochim. Acta.* 64(14), 2479–2488.

721

722 Chiodini, G., Cioni, R., Marini, L., 1993. Reactions governing the chemistry of crater
723 fumaroles from Vulcano Island, Italy, and implications for volcanic surveillance. *Appl.*
724 *Geochem.* 8, 357–371.

725

726 Clayton, R.N., Steiner, A., 1975. Oxygen isotope studies of the geothermal system at
727 Wairakei, New Zealand. *Geochim. Cosmochim. Acta.* 39; 1179-1186.

728

729 Clayton, R.N., Muffler, L.J.P, White, D.E, 1968. Oxygen isotope study of calcite and silicates
730 of the River Ranch well No. I, Salton Sea geothermal field, California. *Am. J. Sci.* 266, 968-
731 979.

732

733 Coplen, T.B., 1988. Normalisation of oxygen and hydrogen isotope data? *Chem Geol Isotope.*
734 72, 293–297.

735

736 Craig, H., 1961. Isotopic variations in meteoric waters. *Science.* 133, 1702-1703.

737

738 Craig, H., 1963. The isotopic geochemistry of water and carbon in geothermal areas. In
739 *Proceedings of the Spoleto Conference on Nuclear Geology* (ed. E. Tongiorgi), pp. 17–53.
740 CNR, Pisa.

741

742 Craig, H., Boat, G., White, D.E., 1956. Isotope geochemistry of thermal waters. *Natl. Acad.*
743 *Sci. Nat. Res. Counc Publ.* 400, 29-39.

744

745 D'Amore, F., Panichi, C., 1980. Evaluation of deep temperature of hydrothermal systems by a
746 new gas-geothermometer. *Geochim Cosmochim Acta.* 44, 549–556.

747

748 Dansgaard, W., 1964. Stable isotopes in precipitation. *Tellus*. 16, 436-467.

749

750 Delorme, H., Verdier, O., Cheminée, J-L., Giret, A., Pineau, F., Javoy, M., 1994. Etude
751 chimique et rapport isotopique du carbone des fumerolles de la Péninsule Rallier du Baty (Iles
752 Kerguelen). *Mém. Soc. Géol. France*. 166, 25–30.

753

754 Duan, Z., Sun, R., 2003. An improved model calculating CO₂ solubility in pure water and
755 aqueous NaCl solutions from 273 to 533 K and from 0 to 2000 bar. *Chem. Geol.* 193, 257-
756 271.

757

758 Duncan, R.A., 2002. A time frame for construction of the Kerguelen Plateau and Broken
759 Ridge. *J. Petrol.* 43 (7), 1109-1120.

760

761 Fischer, T.P., Giggenbach, W.F., Sano, Y., Williams, S.N., 1998. Fluxes and sources of
762 volatiles discharged from Kudryavy, a subduction zone volcano, Kurile Islands. *Earth Planet.*
763 *Sci. Lett.* 160, 81–96.

764

765 Fournier, R.O., 1991. Water geothermometers applied to geothermal energy, In: D'Amore, F.
766 (coordinator). *Application of Geochemistry in Geothermal Reservoir Development*.
767 UNITAR/UNDP publication, Rome, 37-69.

768

769 Fournier, R O., Potter, R.W., 1982. A revised and expanded silica (quartz) geothermometer.
770 Geotherm Resourc Council Bull. 11, 3–12.
771
772 Fournier, R. O., Rowe, J.J., 1966. The deposition of silica in hot springs. Bulletin
773 Volcanologique. 29, 585–587.
774
775 Fournier, R.O., Truesdell, A.H., 1974. Geochemical indicators of subsurface temperature. Part
776 2, estimation of temperature and fraction of hot water mixed with cold water. U.S. Geological
777 Survey Journal of Research. 2 (3), 263–270.
778
779 Frenot, Y., Gloaguen, J-C., Picot, G., Bougère, J., Benjamin, D., 1993. Azorella selago Hook
780 used to estimate glacier fluctuations and climatic history in the Kerguelen Islands over the last
781 two centuries. Oecologia, 95, 140–144.
782
783 Fritz, P., Fontes, J-C., (Eds.) 1986. Handbook of Environmental Isotope Geochemistry. 1st ed.
784 Vol. I, II. and III. The Terrestrial Environment, A. and B. Ed. Elsevier. Scientific Publishing
785 Company. New York. EE.UU. 545-557-428.
786
787 Gagnevin, D., Ethien, R., Bonin, B., Moine, B., Féraud, G., Gerbe, M-C., Cottin, J-Y.,
788 Michon, G., Tourpin, S., Mamias, G., Perrache, C., Giret, A., 2003. Open-system processes in
789 the genesis of silica-oversaturated alkaline rocks of Rallier-du-Baty Peninsula, Kerguelen
790 Archipelago (Indian Ocean). J. Volcanol. Geotherm. Res. 123, 267–300.

791

792 Galley, M.R., Miller, A.I., Atherley, J.F., Mohn, M., 1972. GS process-physical properties:
793 Chalk River, Ontario, Canada. Atomic Energy of Canada Limited, AECL-4225, AECL,
794 Mississauga, ON

795

796 Giggenbach, W.F., 1987. Redox processes governing the chemistry of fumarolic gas
797 discharges from White Island, New Zealand. *Appl Geochem.* 2, 143–161.

798

799 Giggenbach, W.F., 1988. Geothermal solute equilibria. Derivation of Na- K- Mg- Ca
800 geoindicators. *Geochim. Cosmochim. Acta.* 52, 2749-2765.

801

802 Giggenbach, W.F., 1991. Chemical techniques for geothermal exploration, In: *Application of*
803 *Geochemistry in Geothermal Reservoir Development.* D'Amore F. (Ed.), UNITAR, New
804 York, 253-273.

805

806 Giggenbach, W.F., 1992a. Isotopic shifts in waters from geothermal and volcanic systems
807 along convergent plate boundaries and their origin. *Earth Planet. Sci. Lett.* 113, 495–510.

808

809 Giggenbach, W.F., 1992b. Isotopic composition of geothermal water and steam discharges.
810 In: *Application of geochemistry in geothermal reservoir development* (D'Amore F,
811 coordinator), UNITAR-UNDP, 253–273.

812

813 Giggenbach, W.F., 1995. Composition of fluids in geothermal systems of the Taupo Volcanic
814 Zone, New Zealand, as a function of source magma. In: Chudaev K.A. (Ed.), *Water-rock*
815 *Interaction*, 8, 9–12.

816

817 Giggenbach, W.F., Stewart, M.K., 1982. Processes controlling the isotope composition of
818 steam and water discharges from steam vents and steam heated pools in geothermal areas.
819 *Geothermics*. 11, 71-80.

820

821 Giret, A., 1990. Typology, evolution and origin of the Kerguelen plutonic series. *Indian*
822 *Ocean: a review*, *Geol. J.* 25, 239–247.

823

824 Gonfiantini, R., Borsi, S., Ferrara, G., Panichi, C., 1973. Isotopic Composition of Waters from
825 the Danakil Depression (Ethiopia). *Earth Planet. Sci. Lett.* 18, 13-21.

826

827 Grégoire, M., Lorand, J-P., Cottin, J-Y., Giret, A., Mattelli, N., Weis, D., 1997. Xenoliths
828 evidence for a refractory oceanic mantle percolated by basaltic melts beneath the Kerguelen
829 archipelago. *Eur. J. Mineral.* 9, 1085–1100.

830

831 Hattori, K., Muehlenbachs, K., 1980. Marine hydrothermal alteration at a Kuroko ore deposit,
832 Kosaka. Japan, *Contrib. Mineral. Petrol.* 74, 285–292.

833

834 Hedenquist, J.W., Matsuhisa, Y., Izawa, E., White, N.C., Giggenbach, W.F., Aoki, M., 1994.
835 Geology, geochemistry, and origin of high sulfidation Cu-Au mineralization in the Nansatsu
836 district. Japan, Econ. Geol. 89, 1-30.

837

838 Hoefs, J., 1980. Stable Isotope Geochemistry. 2nd edition. 208 pp., 52 figs, 23 tables. Berlin,
839 Heidelberg, New York: Springer-Verlag, ISBN 3 540.

840

841 Horita, J., Wesolowski, D.J. 1994. Liquid-vapor fractionation of oxygen and hydrogen
842 isotopes of water from freezing to the critical temperature. Geochim. Cosmochim. Acta. 58,
843 3425–3437.

844

845 Javoy, M., Pineau, F., Allegre, C.J., 1982. Carbon geodynamic cycle. Nature. 300, 171- 173.

846

847 Lebouvier, M., Laparie, M., Hullé, M., Marais, A., Cozic, Y., Lalouette, L., Vernon, P.,
848 Candresse, T., Frénot, Y., Renault, D., 2011. The significance of the sub-Antarctic Kerguelen
849 Islands for the assessment of the vulnerability of native communities to climate change, alien
850 insect invasions and plant viruses. Biol Invasions. 13, 1195–1208.

851

852 Liebscher, A., Heinrich, C.A., 2007. Fluid-fluid interactions in the Earth's lithosphere. MSA
853 Reviews in Mineralogy and Geochemistry. 65, 430 p.

854

855 Lowenstern, J.B., Janik, C.J., Fahlquist, L., Johnson, L.S., 1999. Gas and isotope
856 geochemistry of 81 steam samples from wells in The Geysers geothermal field, Sonoma and
857 Lake Counties, California, USA. U.S. Geological Survey Open-File Report. 99-304, 28 p.
858 (<http://wrgis.wr.usgs.gov/open-file/of99-304/>).

859

860 Luyendick, B.P., Rennick, W., 1977. Tectonic history of aseismic ridges in the eastern Indian
861 Ocean. *Geol. Soc. Am. Bull.* 88,1347–1356.

862

863 McCrea, J.M., 1950. On the isotopic geochemistry of carbonates and a paleotemperature
864 scale. *J. Chem. Phys.* 18, 849–857.

865

866 Majoube, M., 1971. Fractionnement en oxygène et en deutérium entre l'eau et sa vapeur. *J.*
867 *Chim. Phys.* 68, 1423

868

869 Marini, L., 2004. Geochemical techniques for the exploration and exploitation of geothermal
870 energy. Dipartimento per lo Studio del Territorio e Delle Sue Risorse, Università Degli Studi
871 di Genova, Genova, Italy.

872

873 Mathieu, L., Byrne, P., Guillaume, D., van Wyk de Vries, B., Moine, B., 2011. The field and
874 remote sensing analysis of the Kerguelen Archipelago structure, Indian Ocean. *J Volcanol*
875 *Geotherm Res.* 199, 206–215.

876

877 Moine, B.N., Grégoire, M., O'Reilly, S.Y., Delpech, G., Sheppard, S. M. F., Lorand, J-P.,
878 Renac, C., Giret, A., Cottin, J-Y., 2004. Carbonatite melt in oceanic upper mantle beneath the
879 Kerguelen Archipelago. *Lithos*. 75, 239–252.

880

881 Mook, W.G., Bommerson, J.C., Staverman, W.H., 1974. Carbon isotope fractionation
882 between dissolved bicarbonate and gaseous carbon dioxide. *Earth Planet. Sci. Lett.* 22, 169–
883 176.

884

885 Ohmoto, H., Rye, R.O., 1979. Isotope of sulfur and carbon, in Barnes, H. L. Ed.,
886 *Geochemistry of Hydrothermal deposits*. John Wiley & Sons, p. 509-567.

887

888 Parkhurst, D.L., Appelo, A.A.J., 1999. User's guide to PHREEQC (version 2)—a computer
889 program for speciation, batch-reaction, one-dimensional transport and inverse geochemical
890 modeling. U.S.G.S. Wat. Res. Inv. Report 99- 4259, 312 pp.

891

892 Pichler, T., Veizer, J., 2004. The precipitation of aragonite from shallow-water hydrothermal
893 fluids in a coral reef, Tutum Bay, Ambitle Island, Papua New Guinea. *Chem. Geol.* 207, 31–
894 45.

895

896 Pope, L.A., Hajash, A., Popp, R.K., 1987. An experimental investigation of the quartz, Na- K,
897 Na- K- Ca geothermometers and the effect of fluid composition. *J. Volcanol. Geotherm. Res.*
898 31, 151-161.

899

900 Pope, E.C., Bird, D.K., Arnórsson, S., Fridriksson, Th., Elders, W.A., Fridleifsson, G.Ó.,
901 2009. Isotopic constraints on ice age fluids in active geothermal systems: Reykjanes, Iceland.
902 *Geochim. Cosmochim. Acta.* 73, 4468-4488.

903

904 Renac, C., Kyser, K., Bowden, P., Moine, B., Cottin, J-Y., 2010. Hydrothermal fluid
905 interaction in basaltic lava units, Kerguelen Archipelago (SW Indian Ocean). *Eur. J. Mineral.*
906 22, 215–234.

907

908 Robinson, R., 1973. Sulfur isotopic equilibrium during sulfur hydrolysis at high temperature.
909 *Earth Planet. Sci. Lett.* 18, 443-450.

910

911 Savin, S.M., Lee, M., 1988. Isotopic studies of phyllosilicates. In ‘‘Hydrous Phyllosilicates
912 (Exclusive of Micas)’’. S.W. Bailey, ed. *Rev. Mineral.* 19, 189–219.

913

914 Shaw, A.M., Hilton, D.R., Fischer, T.P., Walker, J., Alvarado, G., 2003. Contrasting volatile
915 systematics of Nicaragua and Costa Rica: Insights to C cycling through subduction zones
916 using He–C relationships. *Earth Planet. Sci. Lett.* 214, 499–513.

917

918 Sheppard, S.M.F., 1986. Characterization and isotopic variations in natural waters. In ‘‘Stable
919 isotopes in high-temperature geological processes’’. J.W. Valley, H.P. Taylor, J.R. O’Neil,
920 eds. *Rev. Mineral.* 16, 165–183.

921

922 Sheppard, S.M.F., Gilg, A., 1996. Stable isotope geochemistry of clay minerals. *Clay*
923 *Minerals*. 31, 1–24.

924

925 Simsek, S., Güleç N., 1994. Geothermal fields of western Anatolia. *International*
926 *Volcanological Congress, Ankara. Excursion, Guide Book*, ISBN 975-429-070-9, IAVCEI-94
927 *Ankara Special Publications*. 8, 1-35.

928

929 Smith, V.R., 2002. Climate change in the sub-Antarctic: an illustration from Marion Island.
930 *Climatic Change*. 52, 345–357.

931

932 Taylor, H.P. Jr., 1979. Oxygen and hydrogen isotope relationships in hydrothermal mineral
933 deposits. In H.L. Barnes, ed., *Geochemistry of Hydrothermal Ore Deposits, Second Edition*:
934 *Wiley and Sons, New York*, 236-277.

935

936 Truesdell, A.H., Hulston, J.R., 1980. Isotopic evidence on environments of geothermal
937 systems. In: Fritz P., Fontes JC. (eds) *Handbook of environmental isotope geochemistry*, vol
938 *I*. Elsevier, New York, Amsterdam, 179–226.

939

940 Vallon, M., 1977. Bilan de masse et fluctuations récentes du glacier Ampère (Iles Kerguelen,
941 TAAF). *Z. Gletscherkd. lazialgeol.* 13, 55– 85.

942

943 Verdier, O., 1989. Champs géothermiques et zéolitisation des îles Kerguelen: implications
944 géologiques (Terres Australes et Antarctiques Françaises, Océan Indien Austral). PhD Thesis,
945 Univ. Paris VI, no 89–29, 269 p.

946

947 Wang, X., Qiao, W., Chen, J., Liu, X., Yang, F., 2018. Understanding the Burial and
948 Migration Characteristics of Deep Geothermal Water Using Hydrogen, Oxygen, and
949 Inorganic Carbon Isotopes. *Water* 2018, 10, 7.

950

951 Watanabe, M., Sakai, H., 1983. Stable isotope geochemistry of sulfates from the Neogene ore
952 deposits in the Green Tuff region. Japan, *Econ Geol Mon.* 5, 282–291.

953

954 Weis, D., Giret, A., 1994. Kerguelen plutonic complexes: Sr, Nd, Pb isotopic study and
955 interferences about their sources, age and geodynamic setting. *Mém. Soc. Géol. France*, 166,
956 47–59.

957

958 Weis, D., Frey, F.A., Leyrit, H., Gautier, I., 1993. Kerguelen Archipelago revisited:
959 geochemical and isotopic study of the southeast Province lavas. *Earth Planet. Sci. Lett.* 118,
960 101–119.

961

962 Weis, D., Frey, F.A., Giret, A., Cantagrel, J.M., 1998. Geochemical characteristics of the
963 youngest volcano (Mounts Cook and Ross) in the Kerguelen Archipelago: interferences for

964 magma flux, lithosphere assimilation and composition of the Kerguelen Plume. *J. Petrol.* 39,
965 973–994.

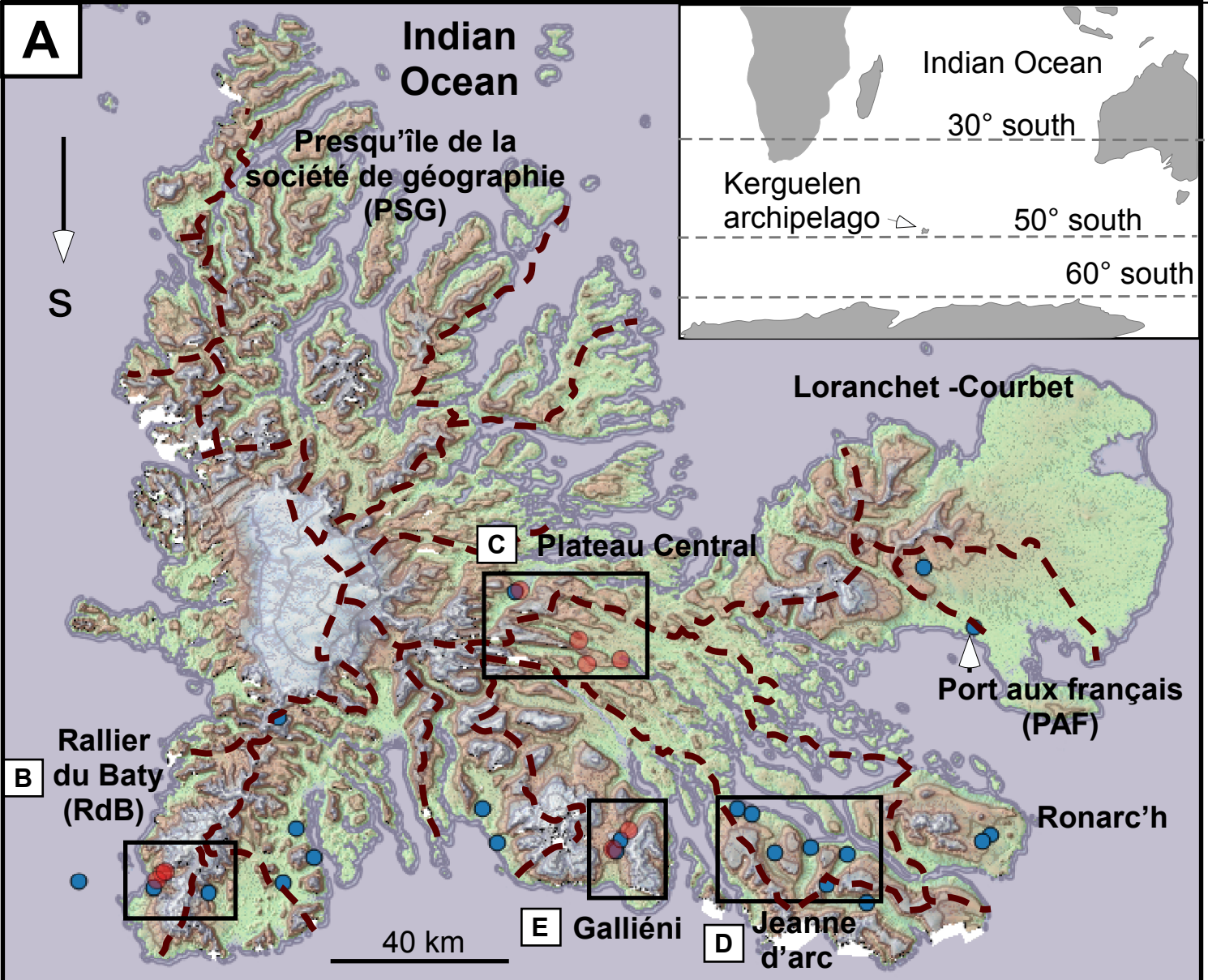
966

967 White, D.E., Muffler, L.P.J., Truesdell, A.H., 1971. Vapor-dominated hydrothermal systems
968 compared with hot water systems. *Econ. Geol.* 66, 75-97.

969

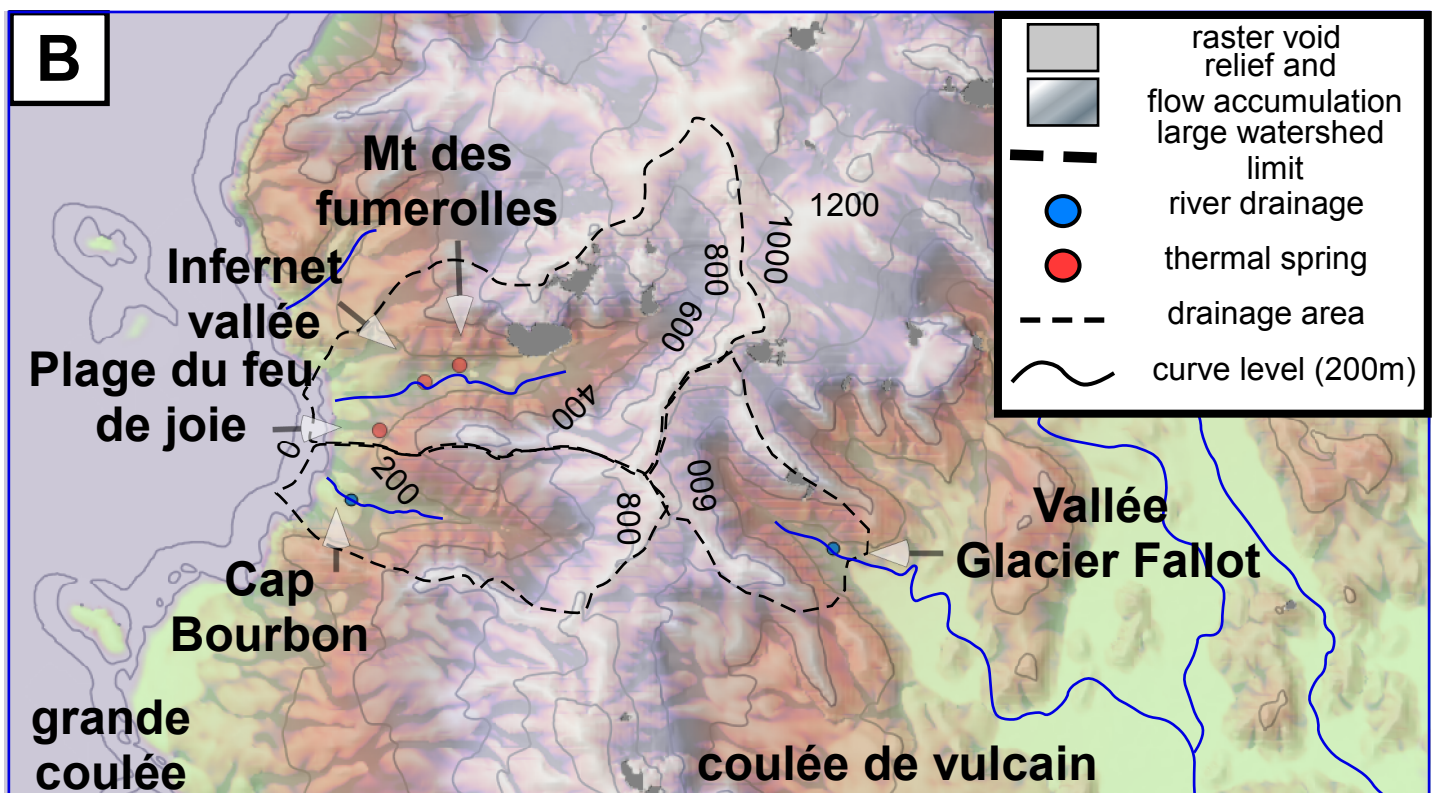
46.6532 S; 46.11983 W

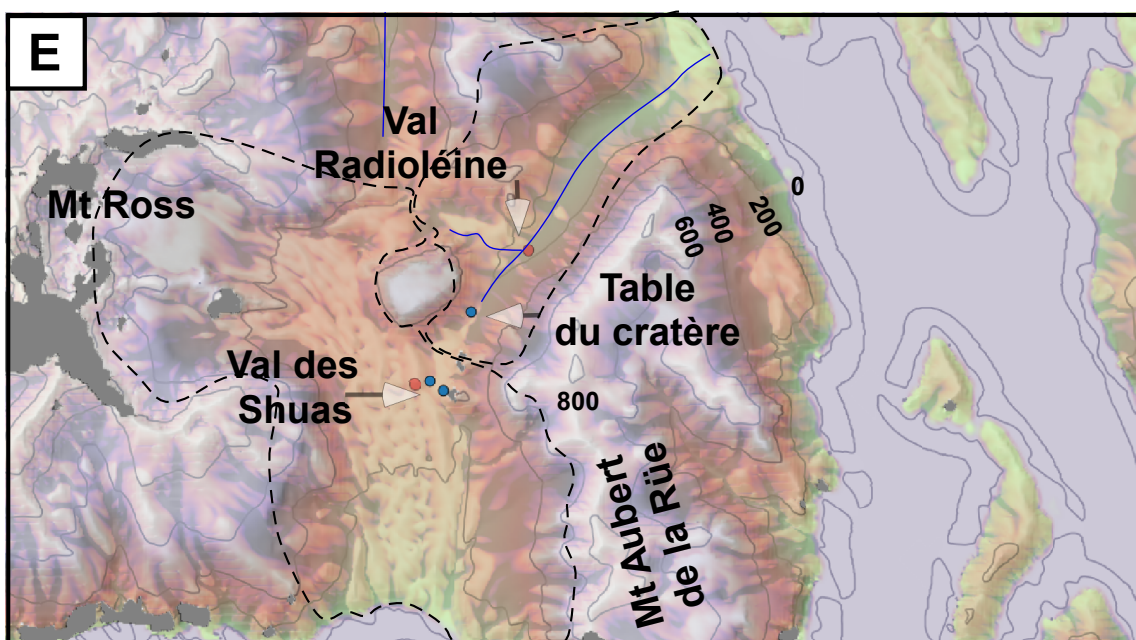
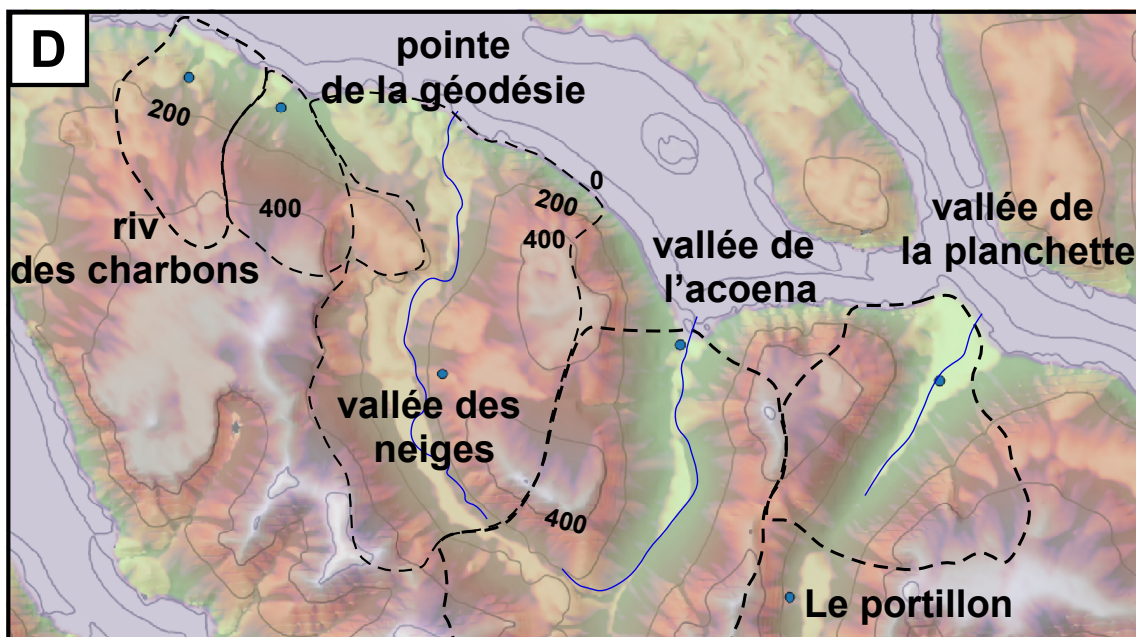
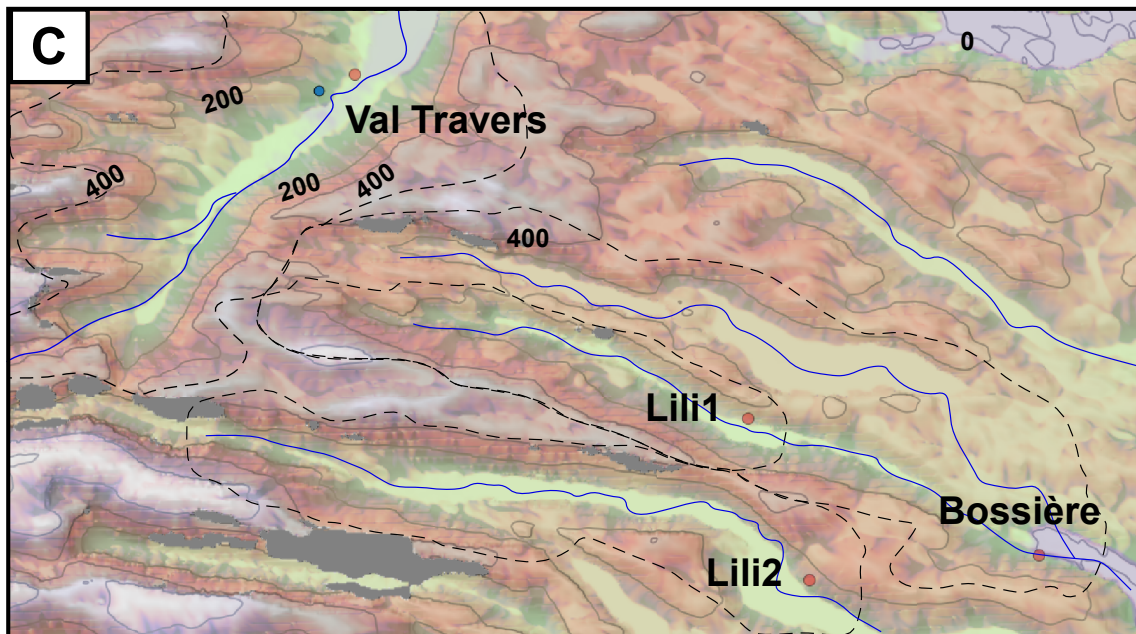
61.7821 S; 46.11983 W



46.6532 S; 44.8835 W

61.7821 S; 44.8835 W





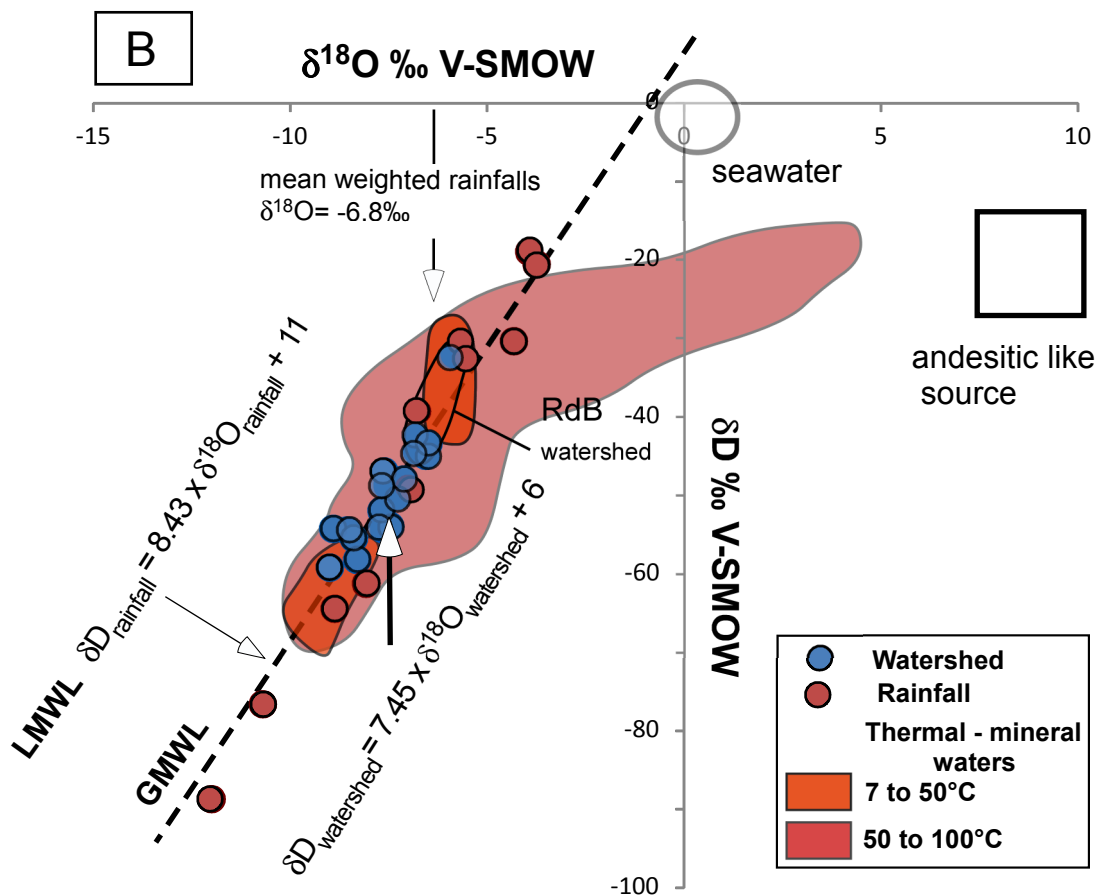
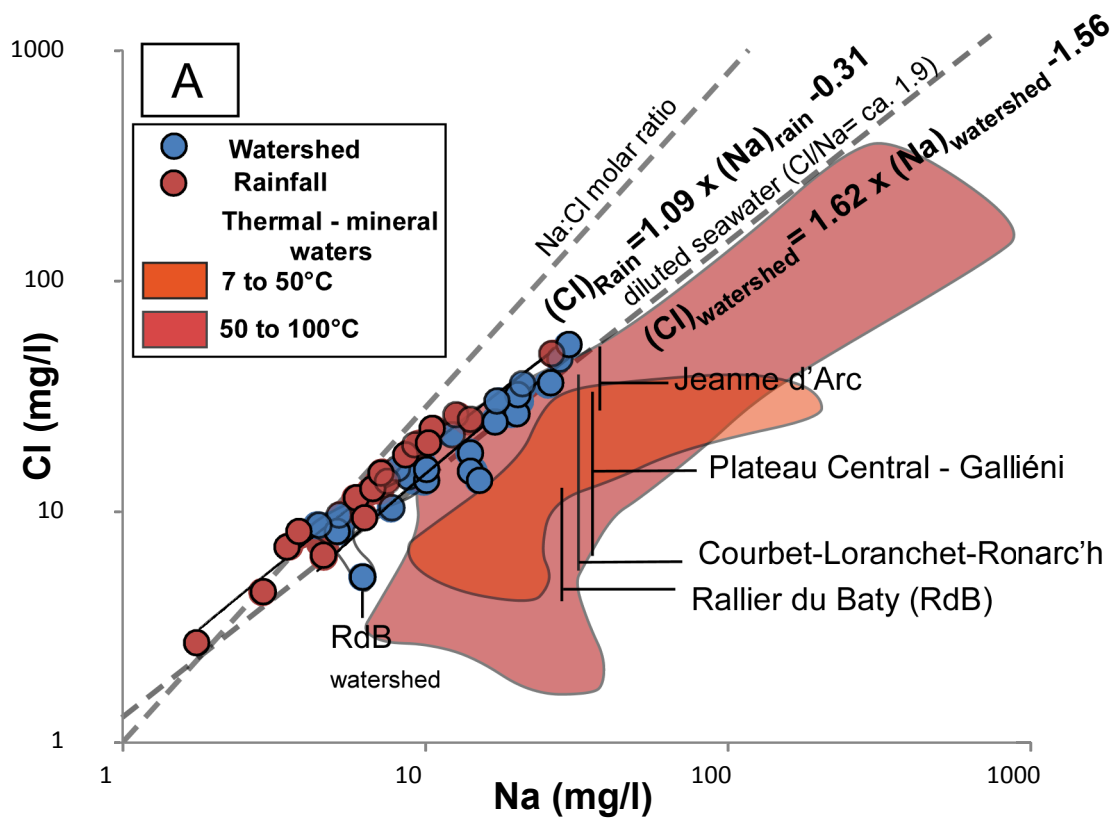
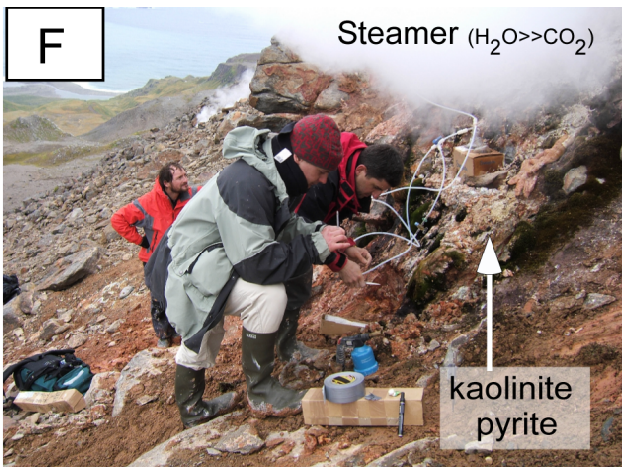
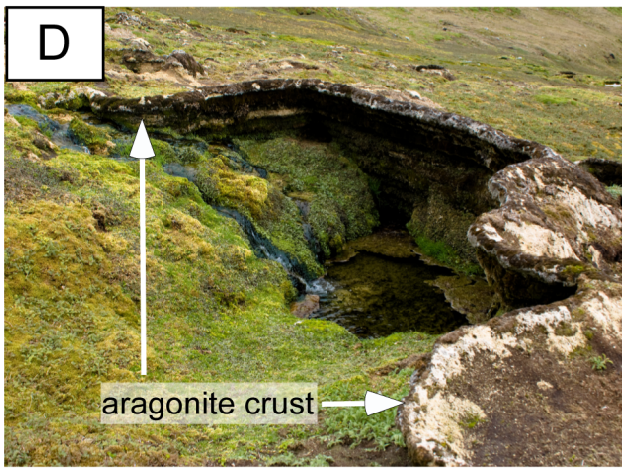
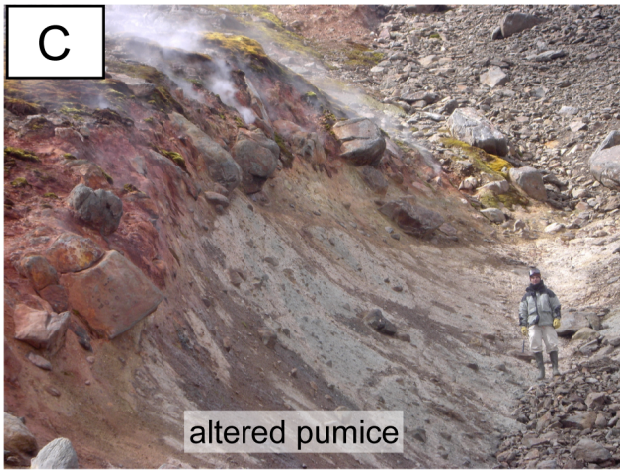
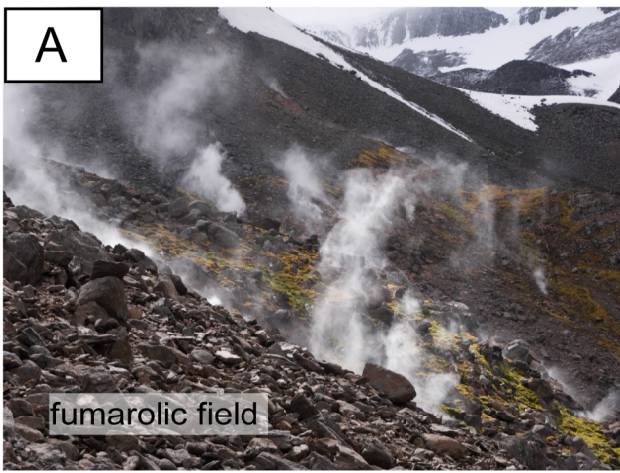


Figure 2



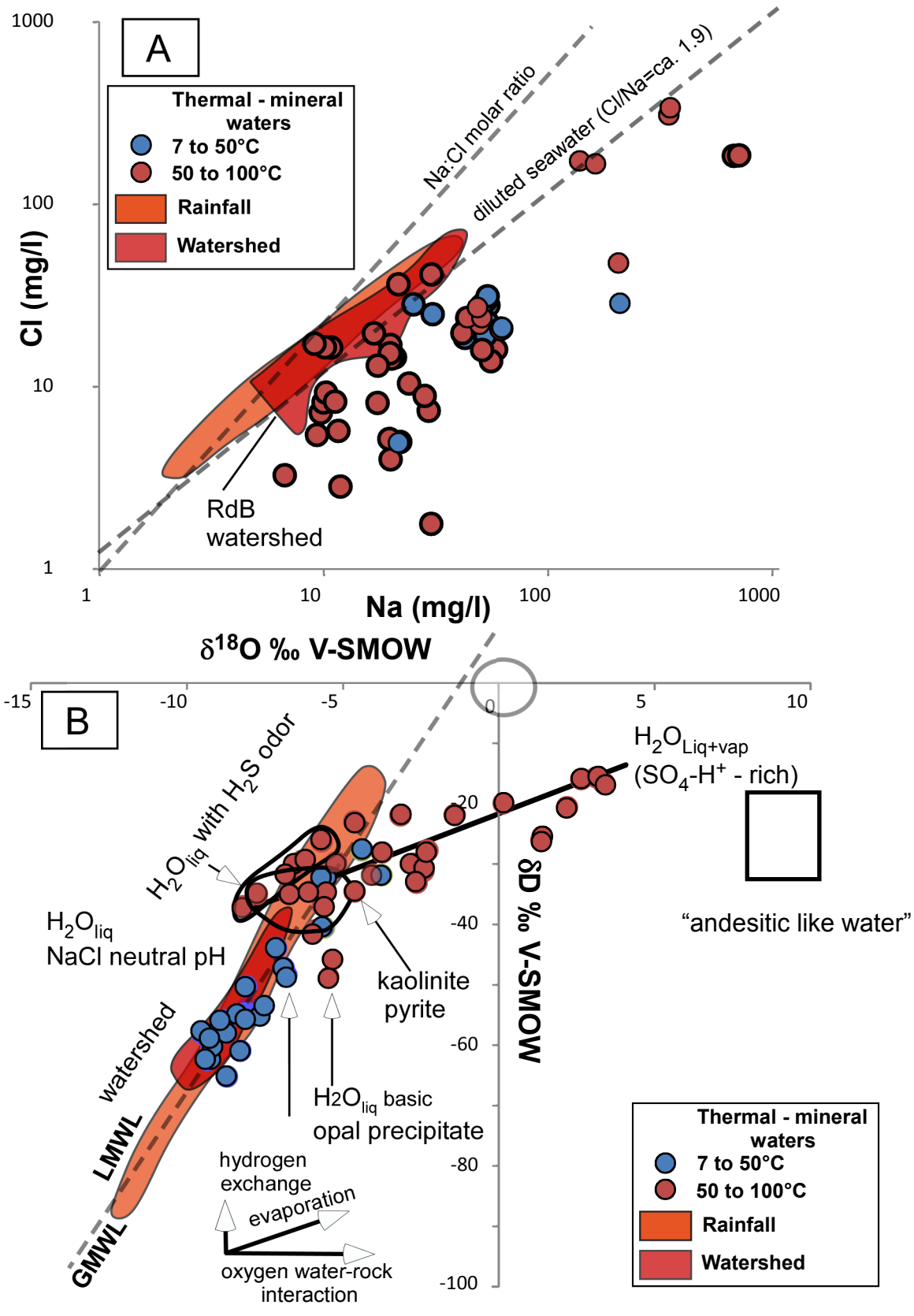


Figure 4

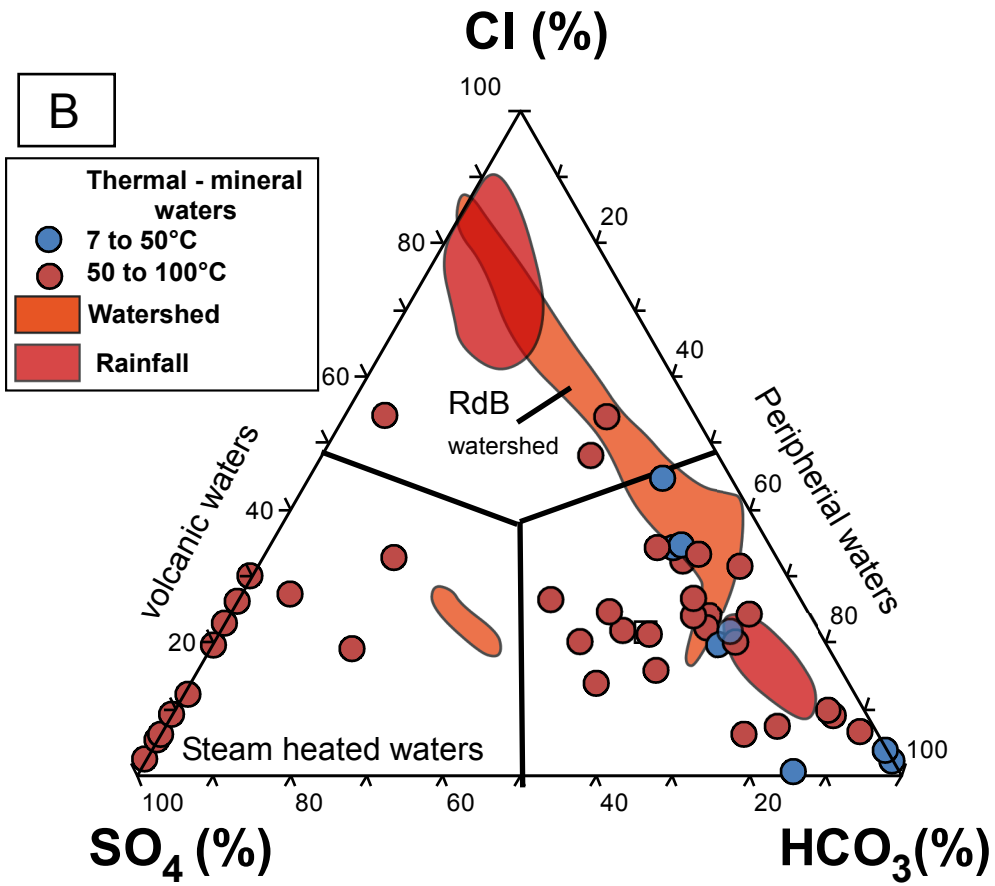
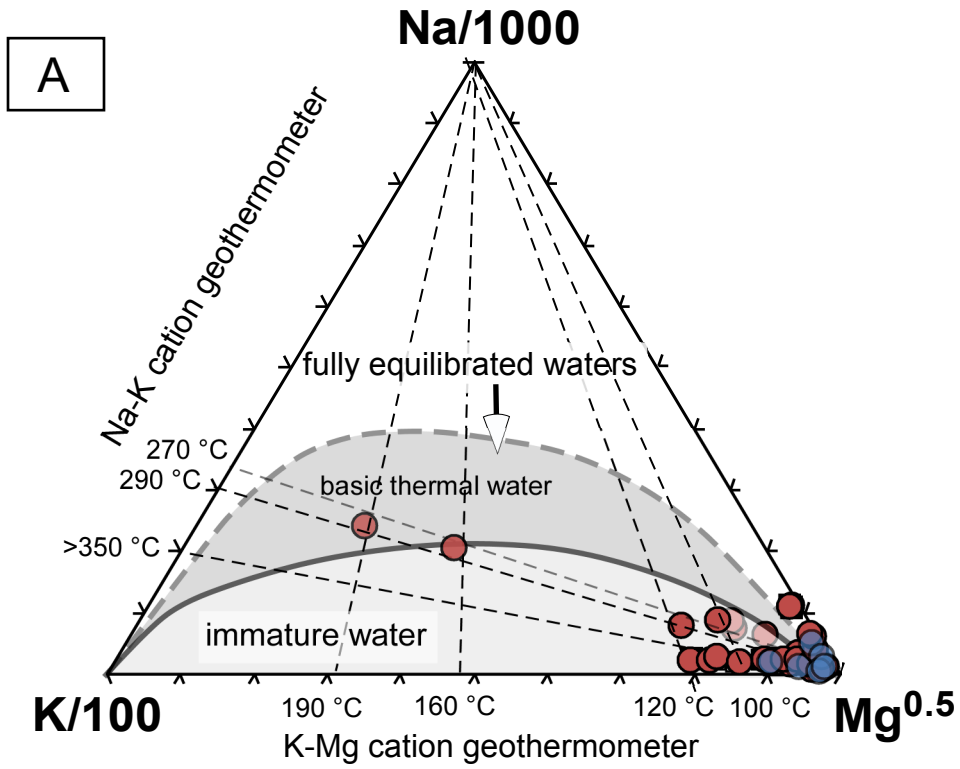


Figure 5

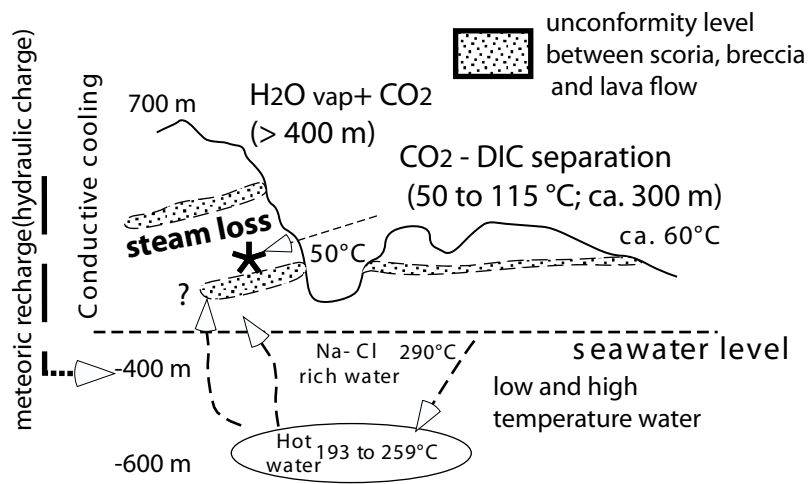


Figure 6

Months	temperature (°C)	rainfall (mm)	c25°C µS/cm	pH	TDS mg/l	Ca mg/l	Mg "	Na "	K "	Cl "	SO ₄ "	NO ₃ "	calculated HCO ₃	δ ¹⁸ O ‰	δD ‰
May 1981	3.7	79	66	n.d.	25	0.28	0.22	7.20	0.25	14.72	2.19	0.03	0	-6.9	-42
June- July	2.5	120	47	"	18	0.16	0.26	5.20	0.18	9.33	2.58	0.04	0	-5.7	-35
Aug-October	n.d.	135	81	"	35	0.60	1.07	10.20	0.42	19.97	2.39	0.04	0	-5.9	-33
Nov-Dec	4.7	105	53	"	21	0.35	0.74	6.24	0.18	9.65	2.19	0.03	2	-10.9	-79
January 1982	7.3	n.d.	38	"	15	0.20	0.42	4.62	0.11	6.38	2.19	0.03	1	n.d.	n.d.
Jan to Feb	7.5	53	83	"	32	0.46	1.46	8.80	0.43	17.84	2.80	0.01	0	-6.9	"
Feb	8.5	45	45	"	32	6.56	0.24	1.80	0.16	2.72	1.80	0.03	19	-8.2	-64
March	7.4	60	75	"	48	7.80	0.72	4.65	0.23	7.08	3.10	0.04	24	-6.7	n.d.
April	5.9	69	230	"	101	8.08	0.78	26.40	1.80	48.20	8.00	0.07	8	-7.2	-51
May	3.9	81	80	"	29	1.82	0.93	7.00	0.48	13.36	2.80	0.02	3	-4.5	-33
June	3.0	70	105	"	37	1.15	1.60	9.60	0.56	19.68	-	0.01	4	-6.4	n.d.
July	2.3	76	64	"	23	1.00	0.87	5.90	0.31	11.44	2.10	0.03	1	-7.0	"
Aug	1.9	70	120	"	40	1.20	1.60	10.60	0.61	22.80	3.60	-	0	-5.6	"
Sept	2.4	72	52	"	17	0.63	0.63	4.70	0.21	8.48	1.80	-	1	-9.0	-67
Oct	3.9	62	80	"	29	0.70	1.27	7.50	0.48	13.84	3.00	0.02	2	-8.4	n.d.
Nov	5.2	61	41	"	15	1.25	0.30	2.90	0.20	4.48	-	-	6	-6.9	"
Dec	6.5	64	49	"	15	0.61	0.60	3.85	0.17	7.92	1.80	-	0	-5.7	"
January 1983	7.8	55	49	"	18	0.55	0.63	4.50	0.24	7.28	2.30	0.01	2	-6.8	n.d.
Feb	8.2	46	120	"	46	1.01	2.07	12.80	0.54	25.92	4.00	0.01	0	-4.1	-22
March	7.2	61	55	"	19	0.49	0.80	5.30	0.23	9.68	1.80	-	1	-3.9	-23
April	6.0	68	116	"	48	0.81	1.87	13.80	0.56	24.64	4.00	-	2	-5.5	n.d.
May	3.2	79	70	"	24	0.45	0.87	7.10	0.43	12.32	2.10	-	1	-12.2	-91
June	2.7	71	68	"	23	0.53	0.93	6.60	0.35	12.24	2.30	0.03	0	-8.7	n.d.
July	2.2	73	42	"	13	0.33	0.48	3.55	0.16	7.06	1.30	-	0	-8.8	"

	Longitude	Latitude	altitude (m)	Temperature (°C)	pH	EC (µS/cm)	Ca mg/l	Mg "	Na "	K "	HCO ₃ "	Cl "	SO ₄ "	NO ₃ "	SiO ₂ "	δ ¹⁸ O ‰	δD ‰
Rallier du Baty																	
Glacier de Plan praz (Riv)	49° 27' 14.73" S	69° 00' 24.89"	41	5	7.10	34	5.00	1.00	6.20	1.13	18.90	5.20	5.40	0.11	4.80	-7.59	-47
Glacier Arago (Riv)	49° 34' 57.31" S	69° 02' 20.35"	7		7.00	31	1.67	0.68	5.20	0.65	8.50	8.20	2.39	0.19	6.80	-6.79	-43
Les 2 frères (Riv)	49° 38' 39.49" S	69° 00' 56.21"	32	16	6.70	47	2.26	0.77	9.20	0.88	8.50	13.60	3.17	0.07	9.40	-6.61	-
Vallée de la Mouche (Riv)	49° 36' 56.82" S	69° 04' 13.61"	23		6.70	51	5.49	1.28	4.90	0.57	9.20	8.70	15.60	0.06	4.40	-6.48	-44
Le portillon (Mt Erebus: Riv)	49° 38' 35.11" S	68° 58' 09.75"	41	7	7.00	26	2.20	0.56	4.40	0.76	6.10	8.70	2.19	0.03	7.60	-6.77	-44
Plateau Central																	
Riv des Tourmentes	49° 18' 41.37" S	69° 25' 13.96"	17	11	7.40	46	4.86	1.35	9.90	0.27	17.70	13.50	4.54	0.06	7.40	-8.89	-54
Tristan lake (end of H. Bossière Fjord)	?	?		18	7.20	57	2.88	0.87	10.00	0.55	9.20	13.70	3.37	0.05	5.80	-7.11	-48
Galléni Massif																	
Plaine de Dante (Riv)	49° 33' 32.15" S	69° 21' 54.34"	62	9	7.30	54	2.67	1.32	14.40	0.82	18.30	15.00	3.17	0.10	6.10	-8.54	-55
Riv au glacier blanc (snow melted)	49° 35' 55.43" S	69° 23' 37.13"	21	2	7.30	45	8.00	1.54	7.70	1.19	18.90	10.30	22.40	0.14	7.30	-8.28	-58
Dianets Lake	?	?		11	7.80	90	5.25	4.34	14.00	1.70	37.20	18.00	5.72	0.07	18.10	-5.73	-32
Val des Skuas (Riv)	49° 36' 16.31" S	69° 35' 49.74"	263	7	7.50	63	4.62	1.09	8.20	1.94	22.60	15.00	3.90	0.07	9.10	-5.81	-32
Val des Skuas (Riv)	49° 36' 21.57" S	69° 36' 02.40"	263	5	6.80	71	4.51	2.34	9.80	3.90	32.90	16.00	4.30	0.04	20.20	-8.97	-59
Table du Cratère (snow melted)	49° 35' 34.03" S	69° 36' 27.29"	228	2	6.60	49	1.69	1.45	15.00	2.13	23.80	13.70	3.37	0.08	14.80		
Courbet Peninsula																	
Port aux Français (water supply: 12/1981)	49° 20' 47.79" S	70° 13' 25.81"	32	6	7.00	94	7.34	4.60	17.50	1.24	32.30	30.00	9.50	0.04	17.50	-7.51	-49
Port aux Français (water supply: 04/1981)	"	"		5	7.30	47	5.46	1.28	12.00	0.52	11.00	22.00	3.95	0.04	5.90	-6.54	-45
Riv du Château (04/1981)	49° 16' 42.14" S	70° 08' 03.88"	111	17	6.70	38	1.16	0.70	5.50	0.66	5.50	9.50	2.18	0.08	1.10	-7.34	-50
Presqu'îles Jeanne d'Arc																	
Riv des Charbons	49° 33' 27.25" S	69° 48' 48.71"	102	8	7.70	80	4.51	2.34	19.20	0.83	18.30	26.50	5.13	0.06	6.20	-7.27	-50
Pte de la Géodésie (Peatbog)	49° 33' 45.29" S	69° 50' 14.36"	56	8	7.70	155	11.90	6.68	27.60	0.93	56.10	46.00	7.88	0.08	12.70	-7.60	-54
Vallée des Neiges (Riv)	49° 35' 23.87" S	69° 52' 46.32"	144	7	7.40	84	5.12	2.94	18.80	0.89	23.20	28.00	4.35	0.13	7.40	-7.25	-50
Vallée de l'Acœna (Riv)	49° 36' 04.16" S	69° 56' 26.09"	5	15	7.40	120	6.21	3.56	20.50	1.04	29.30	30.00	4.54	0.15	11.70	-7.44	-54
Vallée de la Planchette (Riv)	49° 36' 24.32" S	70° 00' 25.58"	17	15	7.60	117	6.49	4.12	17.80	0.92	30.50	29.00	7.49	0.07	12.60	-7.40	-
Vall Levant (Riv)	49° 39' 44.97" S	70° 02' 32.40"	65	14	7.20	120	3.36	2.74	21.00	0.93	16.50	35.00	6.50	0.07	8.60	-	-
Presqu'îles Ronarch'h																	
Riv des Macaronis	49° 34' 54.61" S	70° 15' 25.15"	126	11	7.10	80	2.35	2.10	17.10	2.10	17.10	25.00	5.13	0.07	9.90	-8.36	-56
Nord de la Coupole (Peat bog)	49° 35' 21.56" S	70° 14' 36.38"	193	6	7.10	128	5.22	4.54	25.40	2.05	35.40	35.50	9.25	0.21	13.60	-7.66	-52
Loranchet Peninsula																	
Les Nuageuses (Riv Ile de Croz: 04/1981)	48° 38' 34.41" S	68° 39' 25.07"	23	13	7.30	152	7.31	3.76	29.60	0.71	15.90	52.50	13.57	0.03	0.30	-5.92	-

Location sampling year	sample name and field observation	GPS location	altitude (m)	Temperature (°C)	pH	EC µS/cm	Ca mg/l	Mg	Na	K	Li	NH ₄	HCO ₃	CO ₃	Cl	SO ₄	PO ₄	NO ₃	F	Br	SiO ₂	δ ¹⁸ O ‰	δD ‰	δ ¹³ C _{DIC} ‰	δ ³⁴ S _{SO4} ‰	Na-K geothermometer °C	
RdB (Cap Bourbon; 1982)			25	88	6.1	217	12.82	2.26	21.20	14.08	15.00		47.00		19.50	32.23		0.08			122.1	-7.1	-44				
1982				92	3.5	406	5.84	4.00	29.60	14.92	30.00		0.00		16.00	285.00		0.14			137.3	-3.8	-32				
Vallée du Glacier Fallot (2009)		49° 39'22"S; 68°53'10"E		57	7.3	1578	85.50	54.29	191.80	33.26			1006.00		44.12				3.84				-9.3	-63	-6.3		278
Rallier du Baty																											
2009	Carbonate precipitate; mineral spring	49°40'37"S; 68°54'02"E		15	7.2	1351	34.86	56.76	177.56	34.09			859.00		29.14	0.40			1.99				-8.7	-65	-6.5		292
RdB (Infernet Valley; 2009)		49° 38'02"S; 68° 48'09"E	30	60	7.3	1872	68.83	8.77	294.97	41.41			412.00		310.06	77.75		1.40	17.26	0.25			-6.8	-49	-22.9		249
"		49° 38'04"S; 68°48'04"E	ca. 50	68	6.5	1993	86.18	19.02	294.54	38.15			602.00		256.96	55.75			4.81				-7.6	-54	-7.3		
"		49° 38'08"S; 68°47'40"E	60	68	7.4	340	4.01	0.42	59.38	15.43			152.00		15.74	8.57			1.75						-8.4		
RdB (Feu de Joie beach; 2009)		49° 38'25"S; 68°47'36"E	18	87	3.6	423	12.56	3.94	40.98	10.94					43.85	122.72							-4.4	-28			
"	H ₂ S odour	49° 38'06"S; 68°47'10"E		90	7.5	975	47.30	17.03	115.75	12.30			233.00		140.25	58.49		5.52	0.55					-14.3	11.6		216
"		49° 38'08"S; 68°47'08"E		85	3.2	336	10.70	4.01	37.28	10.57					23.23	98.00							-5.6	-41	-8.4		
"		49° 38'29"S; 68°47'19"E		69	7.5	1102	72.38	10.33	138.25	13.99			369.00		132.22	43.44			2.14	3.24			-8.3	-61	-7.0		211
"		49° 38'38"S; 68°47'13"E		93	6.8	393	24.33	11.61	29.47	4.79			98.00		42.04	37.56							-6.9	-47	-6.5		
RdB (Mont des Fumeroles; 1981)	condensed vapor	49°37'54" S; 68° 47'94" E	ca. 425	72	4.5	361	0.51	1.42	30.30	23.80	0.01				41.00	118.00		0.09			195.3	2.2	-21				
2007	RB1	49°37'54" S; 68° 47'94" E		82	3.5	380	1.15	2.04	30.26	22.80	0.01	0.82			1.77	110.08			0.07								
2007	RB2		ca. 425	100	7.3	83	0.13	0.58	11.67	4.23		n.d.	6.00		5.70	19.13			0.09				2.7	-16			
2007	Condensed vapor (RB 3)		"	97	7.6	88.5	1.06	2.68	10.85	1.21		0.14	12.00		16.34	5.73			0.09				-5.2	-42			
	Condensed vapor (RB 4)		"	87	4	110	0.20	1.34	6.74	5.39		1.26			3.26	43.81			0.02				-5.9	-41	-10.9		
1981	Steamer (native sulfur)		"	95	6.6	153	0.49	1.40	21.60	5.52	<5		3.70		36.20	27.60		0.07			50.7	-2.4	-31	-10.2			
2007	RB5		"	85	7.2	146.8	1.92	5.41	19.90	6.37		0.17	41.00		16.87	19.88			0.20				-2.8	-30			260
2007	Opale precipitate		203	62	10.4	3400	13.50	1.56	673.72	147.96	1.22	8.62	150.00	800.00	183.48	40.34			23.78	0.38	<200	-5.5	-49			"270"	
"	Opale precipitate				10.3	3510	3.83	0.46	711.89	156.21	1.29	0.00	150.00	800.00	184.42	39.59			24.06	0.61			-5.7	-52			"290"
2007	Sue Pt 335		300	50	6.4	965	5.05	1.12	20.85	5.68		0.12	48.00		14.42	10.40			0.38				-5.7	-26			
"	Sue Pt 334			50	7.4	681	178.77	12.95	21.99	1.87	0.01	0.00	650.00		4.96	3.04			0.33				-5.6	-37			193
"	RB5			57	4.5	109	0.67	0.76	9.73	5.21		0.72			7.16	24.44			0.03				3.1	-16			
2007	RB7			70	2.7	341	11.83	5.57	11.94	9.77		4.83			2.82	140.19			0.10				-8.2	-37			
2009				5.1	117		2.29	1.34	9.36	5.78					5.43	37.85							-6.7	-35			
1981	Vapor, H ₂ S odour minor amount of pyrite (RB 5)		ca. 330	95	8.5	123	3.19	0.52	19.80	7.50			38.50	trace	14.70	15.76		0.06			77.8	-6.0	-35				
2007	RB10			82	7.8	168	4.23	0.50	19.71	6.77	0.01	0.00	58.00		5.15	9.03			0.28				-6.3	-29	-5.1		
2009	"			91	7.2	156	4.18	0.47	20.10	7.27			38.00		14.19	12.63			0.47				-6.5	-30	5.5		
1981	-28		ca. 300	61	6.3	123	0.57	0.74	16.80	6.00	<5		9.80		19.50	31.45		0.16			68.1	-2.3	-28				
2007	RB13			73	7.6	145	2.80	0.79	19.80	7.55		0.26	31.00		15.19	16.35			0.26				-2.6	-33			
2009	"			75	7.5	298	3.24	0.36	55.85	8.44			133.00		13.76	8.24			1.77				-2.6	-30			
2007	kaolinite, pyrite and vapor (RB 14)	49°37'54"S; 68°48'48"E	430	98	8.5	147	4.08	0.51	19.96	6.71	0.01	0.00	50.00	4.00	3.98	11.27		0.24	0.24				-4.0	-32	-5.05 to -5.2 (CO ₂)	3.5 (native S)	
2007	RB15			73	8.3	164	2.96	0.28	58.86	8.54	0.03	0.00	132.00	5.00	15.91	8.02			1.53				-4.6	-35	5.5		
2009	"			7.5	298		3.24	0.36	55.85	8.44			133.00		13.76	8.24			1.77				-6.8	-32			259
2007	thermal and watershed (RB18)			65	7.4	83	2.62	1.39	10.14	0.97		0.16	10.00		16.35	3.94	0.14		0.04				-5.2	-30			
2009	"			6.3	68		2.38	1.08	9.13	1.95			12.00		17.10	2.81			0.01				-7.8	-35			
2007	RB21	49°37'36"S; 68° 47'54"E		79	6.9	192	4.01	1.93	24.08	8.80			45.00		10.36	28.69	0.18		0.18				-3.7	-28			9.0
2009	"			91	7	133	1.67	0.45	17.47	7.39			20.00		13.00	16.10			0.65		7.3		-4.9				
2010	"			7.1	120		1.19	0.49	17.42	5.89			31.00		8.11	12.42			0.29				-4.6	-23			
2007	RB32			90	6.7	91	0.77	0.80	10.02	4.71		0.59	2.00		8.17	20.26			0.05				-1.4	-22			
2009	"			6.4	103		2.18	1.32	10.29	5.59					9.24	22.15							-3.2	-22			242
2007	RB35			4.1	103		1.57	0.99	11.30	5.42					8.25	24.23							0.2	-20			
2007	condensed vapor (RB 39)			60	3.5	390	2.01	0.90	29.47	23.43	0.01	1.31			7.36	108.62			0.22				3.4	-17			
2009	"			4	276		2.27	1.03	28.25	22.37					8.87	94.79			0.28				1.4	-26			
Plateau Central (Thermal springs)																											
Val Travers (1981)		49° 18' 31" S; 69°25'47"E	11	61	9.3	250	1.37	0.15	49.80	0.68	<10		30.50	19.80	30.00	15.60		0.04				82.6	8.8	56			
		49° 18' 31" S; 69°25'45"E	11	62	9.4	250	1.38	0.16	48.80	0.62	<10		30.50	19.20	31.50	16.20		0.04				82.2	-8.9	-56			
		49° 18' 31" S; 69°25'45"E	11	60	9.4	241	1.35	0.16	47.30	0.67	<10		29.30	17.40	30.00	16.30		0.04				86.4	-8.8	-56			
2007		"		61	9.5	237	0.79	0.27	49.33	0.68		0.44	72.00		24.42	16.58			0.16								
"		"		61	9.4	222	0.85	0.34	50.09	0.66		0.53	80.00		23.48	14.02			0.14				-8.1	-54	-9.4		
"		"		60	8.1	182.6	0.83	0.55</																			

Months	temperature (°C)	rainfall (mm)	c25°C µS/cm	pH	TDS mg/l	Ca mg/l	Mg "	Na "	K "	Cl "	SO ₄ "	NO ₃ "	calculated HCO ₃	δ ¹⁸ O ‰	δD ‰
May 1981	3.7	79	66	n.d.	25	0.28	0.22	7.20	0.25	14.72	2.19	0.03	0	-6.9	-42
June- July	2.5	120	47	"	18	0.16	0.26	5.20	0.18	9.33	2.58	0.04	0	-5.7	-35
Aug-October	n.d.	135	81	"	35	0.60	1.07	10.20	0.42	19.97	2.39	0.04	0	-5.9	-33
Nov-Dec	4.7	105	53	"	21	0.35	0.74	6.24	0.18	9.65	2.19	0.03	2	-10.9	-79
January 1982	7.3	n.d.	38	"	15	0.20	0.42	4.62	0.11	6.38	2.19	0.03	1	n.d.	n.d.
Jan to Feb	7.5	53	83	"	32	0.46	1.46	8.80	0.43	17.84	2.80	0.01	0	-6.9	"
Feb	8.5	45	45	"	32	6.56	0.24	1.80	0.16	2.72	1.80	0.03	19	-8.2	-64
March	7.4	60	75	"	48	7.80	0.72	4.65	0.23	7.08	3.10	0.04	24	-6.7	n.d.
April	5.9	69	230	"	101	8.08	0.78	26.40	1.80	48.20	8.00	0.07	8	-7.2	-51
May	3.9	81	80	"	29	1.82	0.93	7.00	0.48	13.36	2.80	0.02	3	-4.5	-33
June	3.0	70	105	"	37	1.15	1.60	9.60	0.56	19.68	-	0.01	4	-6.4	n.d.
July	2.3	76	64	"	23	1.00	0.87	5.90	0.31	11.44	2.10	0.03	1	-7.0	"
Aug	1.9	70	120	"	40	1.20	1.60	10.60	0.61	22.80	3.60	-	0	-5.6	"
Sept	2.4	72	52	"	17	0.63	0.63	4.70	0.21	8.48	1.80	-	1	-9.0	-67
Oct	3.9	62	80	"	29	0.70	1.27	7.50	0.48	13.84	3.00	0.02	2	-8.4	n.d.
Nov	5.2	61	41	"	15	1.25	0.30	2.90	0.20	4.48	-	-	6	-6.9	"
Dec	6.5	64	49	"	15	0.61	0.60	3.85	0.17	7.92	1.80	-	0	-5.7	"
January 1983	7.8	55	49	"	18	0.55	0.63	4.50	0.24	7.28	2.30	0.01	2	-6.8	n.d.
Feb	8.2	46	120	"	46	1.01	2.07	12.80	0.54	25.92	4.00	0.01	0	-4.1	-22
March	7.2	61	55	"	19	0.49	0.80	5.30	0.23	9.68	1.80	-	1	-3.9	-23
April	6.0	68	116	"	48	0.81	1.87	13.80	0.56	24.64	4.00	-	2	-5.5	n.d.
May	3.2	79	70	"	24	0.45	0.87	7.10	0.43	12.32	2.10	-	1	-12.2	-91
June	2.7	71	68	"	23	0.53	0.93	6.60	0.35	12.24	2.30	0.03	0	-8.7	n.d.
July	2.2	73	42	"	13	0.33	0.48	3.55	0.16	7.06	1.30	-	0	-8.8	"

	Longitude	Latitude	altitude (m)	Temperature (°C)	pH	EC (μS/cm)	Ca mg/l	Mg "	Na "	K "	HCO ₃ "	Cl "	SO ₄ "	NO ₃ "	SiO ₂ "	δ ¹⁸ O ‰	δD ‰
Rallier du Baty																	
Glacier de Plan praz (Riv)	49° 27' 14.73" S	69° 00' 24.89"	41	5	7.1	34	5.00	1.00	6.20	1.13	18.90	5.20	5.40	0.11	4.80	-7.59	-47
Glacier Arago (Riv)	49° 34' 57.31" S	69° 02' 20.35"	7		7.0	31	1.67	0.68	5.20	0.65	8.50	8.20	2.39	0.19	6.80	-6.79	-43
Les 2 frères (Riv)	49° 38' 39.49" S	69° 00' 56.21"	32	16	6.7	47	2.26	0.77	9.20	0.88	8.50	13.60	3.17	0.07	9.40	-6.61	-
Vallée de la Mouche (Riv)	49° 36' 56.82" S	69° 04' 13.61"	23		6.7	51	5.49	1.28	4.90	0.57	9.20	8.70	15.60	0.06	4.40	-6.48	-44
Le portillon (Mt Erebus; Riv)	49° 38' 35.11" S	68° 58' 09.75"	41	7	7.0	26	2.20	0.56	4.40	0.76	6.10	8.70	2.19	0.03	7.60	-6.77	-44
Plateau Central																	
Riv des Tourmentes	49° 18' 41.37" S	69° 25' 13.96"	17	11	7.4	46	4.86	1.35	9.90	0.27	17.70	13.50	4.54	0.06	7.40	-8.89	-54
Tristan lake (end of H. Bossière Fjord)	?	?		18	7.2	57	2.88	0.87	10.00	0.55	9.20	13.70	3.37	0.05	5.80	-7.11	-48
Galliéni Massif																	
Plaine de Dante (Riv)	49° 33' 32.15" S	69° 21' 54.34"	62	9	7.3	54	2.67	1.32	14.40	0.82	18.30	15.00	3.17	0.10	6.10	-8.54	-55
Riv au glacier blanc (snow melted)	49° 35' 55.43" S	69° 23' 37.13"	21	2	7.3	45	8.00	1.54	7.70	1.19	18.90	10.30	22.40	0.14	7.30	-8.28	-58
Diane's Lake	?	?		11	7.8	90	5.25	4.34	14.00	1.70	37.20	18.00	5.72	0.07	18.10	-5.73	-32
Val des Skuas (Riv)	49° 36' 16.31" S	69° 35' 49.74"	263	7	7.5	63	4.62	1.09	8.20	1.94	22.60	15.00	3.90	0.07	9.10	-5.81	-32
Val des Skuas (Riv)	49° 36' 21.57" S	69° 36' 02.40"	263	5	6.8	71	4.51	2.34	9.80	3.90	32.90	16.00	4.30	0.04	20.20	-8.97	-59
Table du Cratère 'snow melted'	49° 35' 34.03" S	69° 36' 27.29"	228	2	6.6	49	1.69	1.45	15.00	2.13	23.80	13.70	3.37	0.08	14.80		
Courbet Peninsula																	
Port aux Français (water supply; 12/1981)	49° 20' 47.79" S	70° 13' 25.81"	32	6	7.0	94	7.34	4.60	17.50	1.24	32.30	30.00	9.50	0.04	17.50	-7.51	-49
Port aux Français (water supply; 04/1981)	"	"		5	7.3	47	5.46	1.28	12.00	0.52	11.00	22.00	3.95	0.04	5.90	-6.54	-45
Riv du Château (04/1981)	49° 16' 42.14" S	70° 08' 03.88"	111	17	6.7	38	1.16	0.70	5.50	0.66	5.50	9.50	2.18	0.08	1.10	-7.34	-50
Presqu'îles Jeanne d'Arc																	
Riv des charbons	49° 33' 27.25" S	69° 48' 48.71"	102	8	7.7	80	4.51	2.34	19.20	0.83	18.30	26.50	5.13	0.06	6.20	-7.27	-50
Pte de la Géodésie (Peatbog)	49° 33' 45.29" S	69° 50' 14.36"	56	8	7.7	155	11.90	6.68	27.60	0.93	56.10	46.00	7.88	0.08	12.70	-7.60	-54
Vallée des Neiges (Riv)	49° 35' 23.87" S	69° 52' 46.32"	144	7	7.4	84	5.12	2.94	18.80	0.89	23.20	28.00	4.35	0.13	7.40	-7.25	-50
Vallée de l'Acœna (Riv)	49° 36' 04.16" S	69° 56' 26.09"	5	15	7.4	120	6.21	3.56	20.50	1.04	29.30	30.00	4.54	0.15	11.70	-7.44	-54
Vallée de la Planchette (Riv)	49° 36' 24.32" S	70° 00' 25.58"	17	15	7.6	117	6.49	4.12	17.80	0.92	30.50	29.00	7.49	0.07	12.60	-7.40	-
Val Levant (Riv)	49° 39' 44.97" S	70° 02' 32.40"	65	14	7.2	120	3.36	2.74	21.00	0.93	16.50	35.00	6.50	0.07	8.60	-	-
Presqu'îles Ronarc'h																	
Riv des Macaronis	49° 34' 54.61" S	70° 15' 25.15"	126	11	7.1	80	2.35	2.10	17.10	2.10	17.10	25.00	5.13	0.07	9.90	-8.36	-56
Nord de la Coupole (Peat bog)	49° 35' 21.56" S	70° 14' 36.38"	193	6	7.1	128	5.22	4.54	25.40	2.05	35.40	35.50	9.25	0.21	13.60	-7.66	-52
Loranchet Peninsula																	
Les Nuageuses (Riv Ile de Croy; 04/1981)	48° 38' 34.41" S	68° 39' 25.07"	23	13	7.3	152	7.31	3.76	29.60	0.71	15.90	52.50	13.57	0.03	0.30	-5.92	-

Location sampling year	sample name and field observation	GPS location	altitude (m)	Temperature (°C)	pH	EC µS/cm	Ca mg/l	Mg "	Na "	K "	Li "	NH ₄ "	HCO ₃ "	CO ₃ "	Cl "	SO ₄ "	PO ₄ "	NO ₃ "	F "	Br "	SiO ₂ "	δ ¹⁸ O ‰	δD ‰	δ ¹³ C _{DIC} ‰	δ ³⁴ S _{SO4} ‰	Na-K geothermometer °C	
RdB (Cap Bourbon; 1982)			25	88	6.1	217	12.82	2.26	21.20	14.08	15.00		47		19.50	32.23		0.08			122.1	-7.1	-44				
1982				92	3.5	406	5.84	4.00	29.60	14.92	30.00		0		16.00	285.00		0.14			137.3	-3.8	-32				
Vallée du Glacier Fallot (2009)		49° 39'22"S; 68°53'10"E		57	7.3	1578	85.50	54.29	191.80	33.26			1006		44.12				3.84				-9.3	-63	-6.3		278
Rallier du Baty																											
2009	bonate precipitate; mineral sp	49°40'37"S; 68°54'02"E		15	7.2	1351	34.86	56.76	177.56	34.09			859		29.14	0.40			1.99				-8.7	-65	-6.5		292
RdB (Infernet Valley; 2009)		49° 38'02"S; 68° 48'09"E	30	60	7.3	1872	68.83	8.77	294.97	41.41			412		310.06	77.75		1.40	17.26	0.25			-6.8	-49	-22.9		249
"		49° 38'04"S; 68°48'04"E	ca. 50	68	6.5	1993	86.18	19.02	294.54	38.15			602		296.96	55.75			4.81				-7.6	-54	-7.3		
"		49° 38'08"S; 68°47'40"E	60	68	7.4	340	4.01	0.42	59.38	15.43			152		15.74	8.57			1.75						-8.4		
RdB (Feu de Joie beach; 2009)		49° 38'25"S; 68°47'36"E	18	87	3.6	423	12.56	3.94	40.98	10.94					43.85	122.72							-4.4	-28			
"	H ₂ S odor	49° 38'06"S; 68°47'10"E		90	7.5	975	47.32	17.03	115.75	12.30			233		140.25	58.49		5.52	0.55				-5.6	-32	-14.3	11.6	216
"		49° 38'08"S; 68°47'08"E		85	3.2	336	10.70	4.01	37.28	10.57					23.23	98.00							-5.6	-41	-8.4		
"		49° 38'29"S; 68°47'19"E		69	7.5	1102	72.38	10.33	138.25	13.99			369		132.22	43.44			2.14	3.24			-8.3	-61	-7.0		211
"		49° 38'38"S; 68°47'13"E		93	6.8	393	24.33	11.61	29.47	4.79			98		42.04	37.56							-6.9	-47	-6.5		
RdB (Mont des Fumeroles; 1981)	condensed vapor	49°37'54" S; 68° 47'94" E	ca. 425	72	4.5	361	0.51	1.42	30.30	23.80	0.01				41.00	118.00		0.09				195.3	2.2	-21			
2007	RB1	49°37'54" S; 68° 47'94" E		82	3.5	380	1.15	2.04	30.26	22.80	0.01	0.82			1.77	110.08			0.07								
2007	RB2		ca. 425	100	7.3	83	0.13	0.58	11.67	4.23		n.d.	6		5.70	19.13			0.09				2.7	-16			
2007	Condensed vapor (RB 3)		"	97	7.6	88.5	1.06	2.68	10.85	1.21		0.14	12		16.34	5.73			0.09				-5.2	-42			
	Condensed vapor (RB 4)		"	87	4	110	0.20	1.34	6.74	5.39		1.26			3.26	43.81			0.02				-5.9	-41	-10.9		
1981	Steamer (native sulfur)		"	95	6.6	153	0.49	1.40	21.60	5.52	<5		4		36.20	27.60		0.07			50.7	-2.4	-31	-10.2			
2007	RB5		"	85	7.2	146.8	1.92	5.41	19.90	6.37		0.17	41		16.87	19.88			0.20				-2.8	-30			260
2007	Opale precipitate		203	62	10.4	3400	13.50	1.56	673.72	147.96	1.22	8.62	150	800	183.48	40.34			23.78	0.38	<200		-5.5	-49			"270"
"	Opale precipitate				10.3	3510	3.83	0.46	711.89	156.21	1.29	0.00	150	800	184.42	39.59			24.06	0.61			-5.7	-52			"290"
2007	See Pt 335		300	50	6.4	965	5.05	1.12	20.85	5.68		0.12	48		14.42	10.40			0.38				-5.7	-26			
"	See Pt 334			50	7.4	681	178.77	12.95	21.99	1.87	0.01	0.00	650		4.96	3.04			0.33				-5.6	-37			193
"	R35			57	4.5	109	0.67	0.76	9.73	5.21		0.72			7.16	24.44			0.03				3.1	-16			
2007	RB7			70	2.7	341	11.83	5.57	11.94	9.77		4.83			2.82	140.19			0.10				-8.2	-37			
2009					5.1	117	2.29	1.34	9.36	5.78					5.43	37.85							-6.7	-35			
1981	Vapor, H ₂ S odour minor amount of pyrite (RB 5)		ca. 330	95	8.5	123	3.19	0.52	19.80	7.50			39	trace	14.70	15.76		0.06				77.8	-6.0	-35			
2007	RB10			82	7.8	168	4.23	0.50	19.71	6.77	0.01	0.00	58		5.15	9.03			0.28				-6.3	-29	-5.1		
2009	"			91	7.2	156	4.18	0.47	20.10	7.27			38		14.19	12.63			0.47				-6.5	-30			5.5
1981	-28		ca. 300	61	6.3	123	0.57	0.74	16.80	6.00	<5		10		19.50	31.45		0.16				68.1	-2.3	-28			
2007	RB13			73	7.6	145	2.80	0.79	19.80	7.55		0.26	31		15.19	16.35			0.26				-2.6	-33			
2009	"				7.5	298	3.24	0.36	55.85	8.44			133		13.76	8.24			1.77					-30			
2007	kaolinite, pyrite and vapor (R	49°37'54"S; 68°48'48"E	430	98	8.5	147	4.08	0.51	19.96	6.71	0.01	0.00	50	4	3.98	11.27		0.24	0.24				-4.0	-32	5 to -5.2	5 (native S)	
2007	RB15			73	8.3	164	2.96	0.28	58.86	8.54	0.03	0.00	132	5	15.91	8.02			1.53				-4.6	-35			
2009	"				7.5	298	3.24	0.36	55.85	8.44			133		13.76	8.24			1.77				-6.8	-32			259
2007	thermal and watershed (RB18)			65	7.4	83	2.62	1.39	10.14	0.97		0.16	10		16.35	3.94	0.14		0.04				-5.2	-30			
2009	"				6.3	68	2.38	1.08	9.13	1.95			12		17.10	2.81			0.01				-7.8	-35			
2007	RB21	49°37'36"S; 68° 47'54"E		79	6.9	192	4.01	1.93	24.08	8.80			45		10.36	28.69	0.18		0.18			7.3	-3.7	-28			9.0
2009	"			91	7	133	1.67	0.45	17.47	7.39			20		13.00	16.10			0.65				-4.9				
2010	"				7.1	120	1.19	0.49	17.42	5.89			31		8.11	12.42			0.29				-4.6	-23			
2007	RB32			90	6.7	91	0.77	0.80	10.02	4.71		0.59	2		8.17	20.26			0.05				-1.4	-22			
2009	"				6.4	103	2.18	1.32	10.29	5.59					9.24	22.15							-3.2	-22			242
2007	RB35				4.1	103	1.57	0.99	11.30	5.42					8.25	24.23							0.2	-20			
2007	condensed vapor (RB 39)			60	3.5	390	2.01	0.90	29.47	23.43	0.01	1.31			7.36	108.62			0.22				3.4	-17			
2009	"				4	276	2.27	1.03	28.25	22.37					8.87	94.79			0.28				1.4	-26			
Plateau Central (Thermal springs)																											
Val Travers (1981)	1	49° 18' 31" S; 69°25'47"E	11	61	9.3	250	1.37	0.15	49.80	0.68	<10		31	20	30.00	15.60		0.04				82.6	-8.8	-56			
	2	49° 18' 31" S; 69°25'45"E	11	62	9.4	250	1.38	0.16	48.80	0.62	<10		31	19	31.50	16.20		0.04				82.2	-8.9	-56			
	3	49° 18' 31" S; 69°25'45"E	11	60	9.4	241	1.35	0.16	47.30	0.67	<10		29	17	30.00	16.30		0.04				86.4	-8.8	-56			
2007	1	"		61	9.5	237	0.79	0.27	49.33	0.68		0.44	72		24.42	16.58			0.16								
"	2	"		61	9.4	222	0.85	0.34	50.09	0.66		0.53	80		23.48	14.02			0.14				-8.1	-54	-9.4		
"	3	"		60	8.1	182.6	0.83	0.55	49.51	0.68		1.02	75		25.13	15.45			0.11				-8.1	-50			
2010	1	"			8.6	235	2.97	0.53	42.09	0.64			60		26.38	14.22			0.20				-8.4	-54	-9.5		

Geochemical exploration of *geothermal* activity in the Kerguelen archipelago, SW Indian Ocean

C. Renac*, B. Blavoux, B. Moine, M. LeRomancer and Ch. Perrache

This paper described the geothermal water of Kerguelen and its active geothermal system. We reconstruct the meteoric origin, and the hydrothermal processes from chemical and isotopic data of rain water and thermal water. Interpretations indicate series of reactions from 6 up to 260°C and few hundred meters below the surface.

